TRIC-A Channels in Vascular Smooth Muscle Contribute to Blood Pressure Maintenance.

AUTHOR(S):

Yamazaki, Daiju; Tabara, Yasuharu; Kita, Satomi; Hanada, Hironori; Komazaki, Shinji; Naitou, Daisuke; Mishima, Aya; ... Miki, Tetsuro; Iwamoto, Takahiro; Takeshima, Hiroshi

CITATION:

Yamazaki, Daiju ...[et al]. TRIC-A Channels in Vascular Smooth Muscle Contribute to Blood Pressure Maintenance.. Cell metabolism 2011, 14(2): 231-241

ISSUE DATE:

2011-08-03

URL:

http://hdl.handle.net/2433/143634

TRIC-A Channels in Vascular Smooth Muscle Contribute to Blood Pressure Maintenance

(Running title: TRIC Channel and Vascular Tonus)

Daiju Yamazaki[1], Yasuharu Tabara[2], Satomi Kita[3], Hironori Hanada[4], Shinji Komazaki[5], Daisuke Naitou[1], Aya Mishima[1], Miyuki Nishi[1], Hisao Yamamura[6], Shinichiro Yamamoto[1], Sho Kakizawa[1], Hitoshi Miyachi[7], Shintaro Yamamoto[3], Toshiyuki Miyata[4], Yuhei Kawano[4], Kei Kamide[8], Toshio Ogihara[8], Akira Hata[9], Satoshi Umemura[10], Masayoshi Soma[11], Norio Takahashi[12], Yuji Imaizumi[6], Tetsuro Miki[2], Takahiro Iwamoto[3], and Hiroshi Takeshima[1#]

[1]Graduate School of Pharmaceutical Sciences and [7]Institute for Virus Research, Kyoto University, Kyoto 606-8501, Japan

[2]Graduate School of Medicine, Ehime University, Ehime 791-0295, Japan

[3]Faculty of Medicine, Fukuoka University, Fukuoka 814-0180, Japan

[4]National Cerebral and Cardiovascular Center, Osaka 565-8565, Japan

[5]Saitama Medical University, Saitama 350-0495, Japan

[6]Graduate School of Pharmaceutical Sciences, Nagoya City University, Aichi 467-8603, Japan

[8]Graduate School of Medicine, Osaka University, Osaka 565-0871, Japan

[9]Graduate School of Medicine, Chiba University, Chiba 260-8670, Japan

[10]Graduate School of Medicine, Yokohama City University, Kanagawa 236-0004, Japan

[11]School of Medicine, Nihon University, Tokyo 173-8610, Japan

[12]Radiation Effects Research Foundation, Hiroshima 732-0815, Japan

[#]Correspondence: Hiroshi Takeshima

Graduate School of Pharmaceutical Sciences, Kyoto University, Kyoto 606-8501, Japan.

Tel: +81-75-753-4572, Fax: +81-75-753-4605, E-mail: takeshim@pharm.kyoto-u.ac.jp

SUMMARY

TRIC channel subtypes, namely TRIC-A and TRIC-B, are intracellular monovalent cation channels postulated to mediate counter-ion movements facilitating physiological Ca^{2+} release from internal stores. *Tric-a*-knockout mice developed hypertension during the daytime due to enhanced myogenic tone in resistance arteries. There are two Ca^{2+} release mechanisms in vascular smooth muscle cells (VSMCs); incidental opening of ryanodine receptors (RyRs) generates local Ca^{2+} sparks to induce hyperpolarization, while agonist-induced activation of inositol trisphosphate receptors (IP_3Rs) evokes global Ca^{2+} transients causing contraction. *Tric-a* gene ablation inhibited RyR-mediated hyperpolarization signaling to stimulate voltage-dependent Ca^{2+} influx, and adversely enhanced IP_3R-mediated Ca^{2+} transients by overloading Ca^{2+} stores in VSMCs. Moreover, association analysis identified single nucleotide polymorphisms (SNPs) around the human *TRIC-A* gene that increase hypertension risk and restrict the efficiency of antihypertensive drugs. Therefore, TRIC-A channels contribute to maintaining blood pressure, while *TRIC-A* SNPs could provide biomarkers for constitutional diagnosis and personalized medical treatment of essential hypertension.

INTRODUCTION

Ca^{2+} release from the endo/sarcoplasmic reticulum (ER/SR) regulates important cellular functions. Ryanodine receptors (RyRs) expressed in excitable cells and inositol 1,4,5-trisphosphate receptors (IP_3Rs) distributed in almost all types of cells comprise a family of Ca^{2+} release channels that are structurally and functionally distinct from other known ion channels (Fleischer, 2008; Patterson et al., 2004). To regulate separate cellular functions, RyRs and IP_3Rs are activated by different mechanisms and often generate Ca^{2+} signals with distinct spatiotemporal characteristics. For example, in vascular smooth muscle cells (VSMCs), spontaneous RyR opening generates local Ca^{2+} sparks that activate cell-surface Ca^{2+}-dependent K^+ channels leading to hyperpolarization, while agonist-induced IP_3R activation evokes global Ca^{2+} transients, which frequently accompany Ca^{2+} waves and oscillations, inducing contraction (Berridge, 2008; Wellman and Nelson, 2003).

When Ca^{2+} is released from the ER/SR, a negative potential probably arises in the lumen that would disturb subsequent Ca^{2+} release. Therefore, physiological Ca^{2+} release likely requires counter-ion movements to balance ER/SR membrane potential (Meissner, 1983). We have identified TRIC (trimeric intracellular cation) channels that form bullet-shaped homo-trimers to function as monovalent cation channels (Pitt et al., 2010; Yazawa et al., 2007). Recent our studies in mutant embryonic cardiomyocytes, alveolar epithelial cells and skeletal myocytes from knockout mice indicate that TRIC channels act as counter-ion channels facilitating physiological ER/SR Ca^{2+} release (Yamazaki et al., 2009; Zhao et al., 2010). However, the vital roles of TRIC channel subtypes, designated TRIC-A and TRIC-B, still remain to be investigated in various tissues. We report here the essential contribution of TRIC-A channels to SR Ca^{2+} handling in VSMCs for blood pressure (BP) maintenance.

RESULTS AND DISCUSSION

Hemodynamic Abnormalities in *Tric-a*-Knockout Mice

Tric-a-knockout mice are normal in terms of growth, reproduction and motor function (Yazawa et al., 2007). However, skeletal muscle preparations from the knockout mice occasionally generate alternan contractions likely due to incidental SR Ca^{2+} overloading, and also exhibit membranous vacuolation in SR segments (Zhao et al., 2010). On the other hand, telemetric monitoring of hemodynamics (Figure 1A and B) detected high BP and slow heart rate (HR) in the knockout mice even at young-adult stages (8–12 weeks old). Both hypertensive and bradycardiac phenotypes were detected during daytime when sympathetic stimuli are inactivated. The hemodynamic profiles suggested that the knockout mice maintain circadian BP and HR oscillations, and both the phenotypes were eliminated in nighttime when sympathetic outputs are facilitated. Therefore, autonomic controls are probably important in developing the phenotypes. Furthermore, tail-cuff measurements carried out during daytime confirmed these phenotypes in the knockout mice (Figure 1C).

Hypertensive Phenotype in *Tric-a*-Knockout Mice

To survey the mechanism of daytime hypertension in *Tric-a*-knockout mice, we examined pharmacological effects, induced by the submaximal doses of various vasodepressors and evaluated as BP shifts in tail-cuff measurements (Figures 1D and S1). Because resistance vessels are not directly regulated by vagal outputs, as expected, the muscarinic antagonist atropine did not affect the hypertensive phenotype. In response to the α1-antagonist prazosin, which inhibits sympathetic vasoconstriction, *Tric-a*-knockout and control mice showed similar BP reduction. Therefore, when

sympathetic controls are abolished in resistance arteries, *Tric-a*-knockout mice seem to retain the hypertensive phenotype. This assumption was supported by vasodilating responses to the α2-agonist clonidine, which pre-synaptically attenuates sympathetic adrenaline/noradrenaline release. Moreover, inhibitors for various vasoactive factors induced essentially the same effects in both genotypes, suggesting that excessive secretion of endogenous vasopressors is not associated with *Tric-a*-knockout hypertension. It is worthy of note that the Ca^{2+} channel antagonists nicardipine and verapamil exerted potent depressor actions in the knockout mice and canceled the hypertensive phenotype.

Comparable to the manner in which *C19ORF42* lies with *TRIC-A* on the human chromosome (Figure 6A), its ortholog *9130011J15Rik* is adjacent to *Tric-a* in the mouse genome (Figure S2A). In *Tric-a*-knockout mice, the ectopic neomycin-resistance gene is inserted into the 5'-terminal region of the *Tric-a* gene to disrupt the first exon (Yazawa et al., 2007) and could also affect *9130011J15Rik* gene expression, leading to the hypertensive phenotype. However, the involvement of this putative gene was eliminated by our observations. Quantitative RT-PCR analysis detected that *9130011J15Rik* expression was similar in various tissues from the knockout and control mice (Figure S2B and C). Moreover, transgenic mice expressing TRIC-A channels under the control of the α-smooth muscle actin promoter were generated and bred with *Tric-a*-knockout mice (Figure S2D–H). The *Tric-a* transgene was abundantly expressed in tissues containing SMCs and rescued hypertension developed under *Tric-a*-knockout conditions. The hypertension-rescue mice, together with remarkable vasodilation induced by Ca^{2+} channel antagonists in *Tric-a*-knockout mice, suggest that abnormalities in SMCs expressing L-type Ca^{2+} channels are primarily responsible for the pathogenesis of the hypertensive phenotype.

Bradycardiac Phenotype in *Tric-a*-Knockout Mice

When atropine and the β1-antagonist metoprolol were co-administered to inhibit autonomic controls to the heart, tail-cuff measurements detected similar intrinsic HRs between *Tric-a*-knockout and control mice (Figure 1C), suggesting normal pacemaking in the mutant hearts. In single-agent administration, atropine remarkably elevated HR to cancel the bradycardiac phenotype, while the heart-slowing metoprolol maintained the phenotype in the knockout mice. Therefore, vagal hyperactivity during daytime is the direct cause of the bradycardiac phenotype. Predominant sympathetic stimuli probably prevent this phenotype during nighttime.

The Rho kinase inhibitor Y27632, α1-antagonist prazosin, angiotensin II AT1-receptor blocker candesartan and Ca^{2+} channel antagonists primarily act in vessels. These vessel-targeted depressors obviously attenuated the bradycardiac phenotype in *Tric-a*-knockout mice (Figure S1), indicating that vagal hyperactivity is induced by baroreceptor reflexes activated under hypertensive conditions. Therefore, baroreflex-mediated vagal hyperactivity, together with sympathetic inactivation during daytime, probably promotes the bradycardiac phenotype in the knockout mice. However, the phenotype was not canceled in the hypertension-rescue mice bearing the SMC-specific *Tric-a* transgene (Figure S2H). Although the rescue mice possess a highly artificial genetic feature, this observation may suggest that neuronal defects, together with activated baroreflexes, take part in vagal hyperactivity. Atypical autonomic activity in the knockout mice is presumed from another side and discussed elsewhere (see the section “Mechanism of *Tric-a*-Knockout Hypertension”).

Elevated MyogenicTone in *Tric-a*-Knockout Artery

Because the *in vivo* experiments suggested that hypertension is a primary defect in *Tric-a*-knockout mice, we next focused on the mutant vessels. Elevation of intravascular pressure causes constriction

of VSMCs in resistance arteries, and this behavior, known as myogenic tone, is a key element for BP maintenance (Segal, 1994). The mesenteric artery, a typical resistance vessel, was cannulated with micropipettes to measure its diameter under a video-monitored perfusion system. Despite showing normal passive diameters in a Ca^{2+}-free bathing solution (Figure S3A–C), *Tric-a*-knockout arteries had narrower diameters at the intraluminal pressure levels examined when compared with control arteries (Figure 2A). Therefore, spontaneous myogenic tone was significantly elevated in the mutant arteries (Figure 2B), and this abnormality seems to directly develop hypertension in *Tric-a*-knockout mice. Spontaneous myogenic tone may be broadly elevated throughout the vascular system of the knockout mice, because isometric tension measurements detected elevated resting tone in aortic ring preparations from *Tric-a*-knockout mice (Figure S4C–F). On the other hand, normal morphology and gene expression were observed in the mutant vessels (Figure S3D and E), suggesting no vascular remodeling in *Tric-a*-knockout mice. Moreover, in the hypertension-rescue mice, the SMC-specific *Tric-a* transgene restored elevated myogenic tone developed under *Tric-a*-knockout conditions to normal levels (Figure 2C).

In response to acetylcholine, the vasorelaxation factors, nitric oxide (NO) and unidentified endothelium-derived hyperpolarizing factor (EDHF), are produced in endothelial cells, and their vasodilating effects can be evaluated using inhibitors attenuating either signaling pathway (Busse et al., 2002; Koshita et al., 2007). Although acetylcholine-induced relaxation was obviously facilitated likely due to elevated spontaneous myogenic tone in *Tric-a*-knockout arteries, fractional rates of NO- and EDHF-dependent relaxation were similar between the mutant and control arteries (Figure S4A and B). Therefore, it is rather unlikely that insufficient vasorelaxation signaling in endothelial cells underlies *Tric-a*-knockout hypertension.

Abnormal Ca^{2+}-Handling in *Tric-a*-Knockout VSMCs

Vascular tonus is controlled by the contraction of VSMCs primarily regulated by intracellular Ca^{2+} signaling (Segal, 1994). NO and EDHF syntheses also depend upon Ca^{2+} signaling in endothelial cells (Busse et al., 2002). RT-PCR detected co-expression of *Tric-a* and *Tric-b* mRNAs in VSMCs and endothelial cells (Figure S5A and B), providing the possibility that TRIC-A channel deficiency may affect both cell types. In Fura-PE3 ratiometric Ca^{2+} imaging of mesenteric arteries lacking endothelial cells, we detected irregular Ca^{2+} handling in *Tric-a*-knockout VSMCs, which were categorized into three abnormalities as described below. In contrast, *Tric-a*-knockout endothelial cells in primary culture retained normal Ca^{2+}-handling properties (Figure S5C–I).

The first abnormality of *Tric-a*-knockout VSMCs was the elevation of resting intracellular Ca^{2+} concentration ($[Ca^{2+}]i$). Elevated resting $[Ca^{2+}]i$ was attenuated by Ca^{2+}-free bathing solutions and verapamil (Figure 2D), while inhibitors of Orai and TRP channels (Smyth et al., 2006) were ineffective (Figure S4I–L). The L-type Ca^{2+} channel agonist BayK8644 remarkably increased resting $[Ca^{2+}]i$ in control VSMCs, but not in the mutant VSMCs (Figure 2E). Therefore, enhanced steady-state Ca^{2+} influx through L-type Ca^{2+} channels probably elevates resting $[Ca^{2+}]i$ in the mutant VSMCs. This assumption was confirmed by the observations that verapamil-sensitive Mn^{2+} influx was significantly facilitated and Mn^{2+} influx was insufficiently activated by BayK8644 in the mutant VSMCs (Figure S6A–C). The proposed hyperactivation of L-type Ca^{2+} channels was not caused by increased channel density or altered channel gating (Figure S6D and E). Moreover, elevated resting $[Ca^{2+}]i$ and enhanced L-type Ca^{2+} channel currents were also indicated in aortic SMCs from the knockout mice (Figure S4G and H). In the hypertension-rescue mice, the SMC-specific transgene reset elevated resting $[Ca^{2+}]i$ induced under *Tric-a*-knockout conditions (Figure 2E).

The second abnormality was SR Ca^{2+}-overloading, as Ca^{2+} leak responses evoked by the ER/SR Ca^{2+}-pump inhibitor cyclopiazonic acid were obviously enhanced in *Tric-a*-knockout VSMCs (Figure 2F and G). SMCs contain distinct Ca^{2+} stores equipped with either RyRs or IP_3Rs, called caffeine- and IP_3-sensitive stores respectively, that partially overlap and functionally interact (Berridge, 2008). Caffeine-sensitive stores were not overloaded in *Tric-a*-knockout VSMCs, because the RyR activator caffeine induced similar transients in the mutant and control cells (Figure 2H and I). The third abnormality was in facilitated agonist-induced Ca^{2+} release; the α1-agonist phenylephrine evoked enhanced IP_3R-mediated Ca^{2+} transients in *Tric-a*-knockout VSMCs (Figure 2J and K). In the mutant VSMCs, normal Ca^{2+} release was induced by caffeine immediately after enhanced phenylephrine-evoked transients under Ca^{2+}-free conditions (Figure 2L and M). Therefore, the *Tric-a* deficiency probably induces Ca^{2+} overloading specifically in IP_3-sensitive stores. Because submicromolar $[Ca^{2+}]i$ potentiates IP_3R activation (Iino, 1990), the enhanced driving force of the overloaded luminal Ca^{2+}, together with elevated resting $[Ca^{2+}]i$, likely facilitate IP_3R-mediated responses in the mutant VSMCs.

Impaired Hyperpolarization Signaling in *Tric-a*-Knockout VSMCs

In SMCs, incidental RyR activation generates Ca^{2+} sparks (Cheng and Lederer, 2008; Nelson et al., 1995) and evokes spontaneous transient outward currents (STOCs) (Ohi et al., 2001; Wray and Burdyga, 2010). High-speed fluorometric imaging detected Ca^{2+} sparks with regular amplitudes generated at hot spots in single *Tric-a*-knockout VSMCs (Figure 3A–D). However, the frequency of Ca^{2+} sparks was noticeably reduced in the mutant cells perfused with a high-K^+ solution. On the other hand, among the three major types of Ca^{2+}-dependent K^+ channels classified using specific inhibitors (Wei et al., 2005), iberiotoxin-sensitive big-conductance (BK) channels predominantly

mediated STOCs in VSMCs from mesenteric arteries (Figure S6F). In patch-clamp recording, *Tric-a*-knockout VSMCs exhibited reduced STOC frequency at high membrane potentials (Figure 3E and F), but they nonetheless retained normal STOC amplitudes (Figure 3G), cell-surface BK channel density and gating feature (Figure S6G and H). Since the reduced STOC frequency is fully consistent with the insufficient spark generation, hyperpolarization signaling generated by functional coupling between RyRs and BK channels is probably compromised in *Tric-a*-knockout VSMCs. Meanwhile, weak Ca^{2+} sparks and STOCs just above the detection limits are always observed in the measurements, but cannot be generally evaluated in the statistical analyses. Although our measurements showed no differences between the genotypes in a normal bathing solution, such miniature events might be insufficiently evoked under resting conditions and steady-state excitability could be altered in *Tric-a*-knockout VSMCs.

Enhanced Excitability in *Tric-a*-Knockout VSMCs

In confocal-microscopic imaging in the continuous presence of the voltage-dependent dye oxonol VI, depolarization results in accumulation of the dye into cells to subsequently increase cellular fluorescence intensity (Apell and Bersch, 1987). The intensity monitored was normalized to the maximum value in a 140 mM KCl bathing solution to yield a fractional intensity (F/F_{140K}) as an index of membrane potential (Figure 4A). In a normal bathing solution, an increased fractional intensity was detected in *Tric-a*-knockout VSMCs, demonstrating the elevation of resting membrane potential (Figure 4B). To analyze the relationship between the fractional intensity and membrane potential, intensity shifts were monitored in several high K^+-bathing solutions and the membrane potentials were estimated by the Nernst equation. Direct microelectrode measurements have determined a resting membrane potential of -59.9 ± 3.0 mV in VSMCs from mouse mesenteric

arteries (Koshita et al., 2007). The prepared calibration plot estimated a resting membrane potential of -54.6 ± 1.7 mV in *Tric-a*-knockout VSMCs (Figure 4C). BK channel blockage with iberiotoxin markedly elevated resting potential in control VSMCs, but not in *Tric-a*-knockout cells (Figure 4D). Additionally, a BK channel opener notably induced vasodilation in the mutant mesenteric arteries, but not in control arteries (Figure S4A). Therefore, BK channel-mediated STOCs take part in maintaining resting membrane potential in VSMCs and spontaneous tonus in resistance arteries, but this mechanism is probably impaired in *Tric-a*-knockout arteries. This conclusion is confirmed by the hypertension-rescue mice; the poor sensitivity to iberiotoxin and elevated resting potential were restored by the SMC-specific *Tric-a* transgene (Figure 4B and D).

We also examined the repolarizing phase of VSMCs after 60 mM KCl-induced depolarization. *Tric-a*-knockout VSMCs showed prolonged repolarizing phases in a normal bathing solution, while the mutant and control VSMCs exhibited similar repolarization in the presence of iberiotoxin (Figure 4E and F). Therefore, BK channels contribute to accelerating repolarization as well as maintaining resting potential in VSMCs. In *Tric-a*-knockout VSMCs, insufficient STOCs likely prolong both depolarizing durations and L-type Ca^{2+} channel opening events.

Mechanism of *Tric-a*-Knockout Hypertension

In SMCs, persistent Ca^{2+} influx through L-type channels seems to maintain resting $[Ca^{2+}]i$ and may refill intracellular stores for further release processes without direct activation of SR Ca^{2+} release (Amberg et al., 2007; Berridge, 2008). Based on the poor Ca^{2+} spark generation in *Tric-a*-knockout VSMCs (Figure 3), we propose that TRIC-A channels primarily facilitate RyR-mediated Ca^{2+} release by providing counter-ion movements across the SR membrane in VSMCs (Figure 5). Because the compromised Ca^{2+} sparks evoke insufficient STOCs (Figure 3), resting membrane

potential is elevated and depolarization is prolonged in *Tric-a*-knockout VSMCs (Figure 4). Under such 'sensitized' conditions, L-type Ca^{2+} channels are hyperactivated causing elevated resting $[Ca^{2+}]i$ in the mutant VSMCs and enhancing myogenic tone in the mutant vessels (Figures 2, S4 and S6). The proposed pathogenic mechanism is consistent with the observations that *Tric-a*-deficient hypertension is highly sensitive to Ca^{2+} channel antagonists (Figure 1), and that the SMC-specific *Tric-a* transgene in the hypertension-rescue mice restored key defects developed under *Tric-a*-knockout conditions (Figures 2 and 4). In addition to the poor Ca^{2+} spark generation, TRIC-A channel deficiency produced Ca^{2+}-overload in the SR and adversely potentiated IP_3R-mediated Ca^{2+} release in VSMCs (Figure 2). Therefore, facilitated agonist-induced Ca^{2+} transients in response to sympathetic stimuli also could elevate vascular tonus. However, this mechanism may not obviously contribute to *Tric-a*-knockout hypertension, because prazosin induced similar vasodilatation in the knockout and control mice (Figure 1).

Tric-a-knockout mice developed both hypertension and bradycardia under the control of the autonomic nervous system (Figure 1). While impaired hyperpolarization signaling in VSMCs continuously elevates spontaneous vascular tonus, hypertension was masked during nighttime in the knockout mice. Therefore, it may be that sympathetic activity of *Tric-a*-knockout mice is adjusted lower during nighttime compared to that of control mice. However, this presumption may conflict with our HR monitoring observations. As discussed above, daytime bradycardia seems to be mainly due to baroreflex-mediated vagal hyperactivity. During nighttime, normal sympathetic and vagal activities are reasonably proposed in the knockout mice, based on their regular HRs under normotensive conditions. The discrepancy between sympathetic activities proposed on the basis of BP and HR monitoring cannot be explained by the baroreflex depression, in which baroreflex sensitivity becomes attenuated as hypertension progresses. Although the pharmacological responses

and circadian hemodynamic profiles suggest that the central autonomic system is regularly functioning in the knockout mice, *Tric-a* gene ablation could induce mild autonomic imbalance to generate aberrant stimuli of targeted tissues. For example, TRIC-A channel deficiency might impair cellular functions in certain pre- or post-ganglionic neurons of the peripheral autonomic system, since TRIC channel subtypes are co-expressed in neurons (Yazawa et al., 2007). In addition to elevated vascular tonus as an absolute predisposing risk for hypertension, aspects of autonomic imbalance might contribute to the atypical hemodynamic features observed in *Tric-a*-knockout mice.

Preferential Coupling between RyR and TRIC-A Channels in VSMCs

In cardiomyocytes, RyRs are abundantly expressed in the SR, while IP_3Rs presumably reside in perinuclear regions at low expression levels. Resulting caffeine- and IP_3-sensitive stores seem to contribute to distinct Ca^{2+} signals regulating contraction and gene expression, respectively (Kockskämper et al., 2008). Knockout mice lacking both TRIC channel subtypes exhibit embryonic heart failure, and the mutant cardiomyocytes show compromised RyR-mediated Ca^{2+} release (Yazawa et al., 2007). Meanwhile, *Tric-a*-knockout and *Tric-b*-knockout mice undergo normal embryonic development, indicating that TRIC channel subtypes possess compatible functions in embryonic cardiomyocytes. However, in other cell types, subtype-specific coupling may be flexibly formed between Ca^{2+} release and TRIC channels. In alveolar type II epithelial cells, agonist-induced Ca^{2+} release stimulates the synthesis and secretion of surfactant phospholipids for lung expansion. *Tric-b*-knockout mice exhibit neonatal lethality due to respiratory failure, and the mutant alveolar type II cells show impaired IP_3R-mediated Ca^{2+} release and insufficiently deal with surfactants (Yamazaki et al., 2009). In this case, functional coupling between IP_3Rs and TRIC-B channels is set

by the gene expression profile; alveolar epithelial cells contain IP_3Rs and TRIC-B channels, but expressions of RyRs and TRIC-A channels are undetectable. In skeletal muscle, RyRs and TRIC-A channels are abundantly distributed in the SR, while IP_3Rs and TRIC-B channels are expressed at low levels. In *Tric-a*-knockout skeletal muscle, Ca^{2+} overloading and membranous vacuolation are developed in the SR likely due to compromised RyR-mediated Ca^{2+} release (Zhao et al., 2010). Although the abnormalities suggest selective coupling between RyRs and TRIC-A channels, it may be superficially formed according to predominant expression of TRIC-A channels. In contrast, VSMCs equip caffeine- and IP_3-sensitive stores roughly equivalent in Ca^{2+} content (Figure 2) and contain *Tric-a* and *Tric-b* mRNAs at similar levels (Figure S5). Insufficient Ca^{2+} sparks and facilitated IP_3R-mediated Ca^{2+} release in *Tric-a*-knockout VSMCs (Figures 2 and 3) clearly suggest preferential coupling between RyRs and TRIC-A channels, and reversely may further presume another coupling between IP_3Rs and TRIC-B channels. However, the mechanism underlying the proposed subtype-selective coupling is unknown, and direct interaction between RyRs and TRIC channels was not detected in crosslinking experiments using skeletal muscle SR preparations (unpublished observation). The proposed coupling could be caused by restricted residency of TRIC channel subtypes in caffeine- or IP_3-sensitive stores, and/or distinct channel characteristics electrophysiologically detected between the subtypes (Pitt et al., 2010).

Even though TRIC-A channel deficiency inhibits RyR-mediated Ca^{2+} release, *Tric-a*-knockout VSMCs developed Ca^{2+}-overloaded IP_3-sensitive stores (Figure 2). This unexpected abnormality may predict the existence of 'Ca^{2+} laundering' between caffeine- and IP_3-sensitive stores. For example, Ca^{2+} pumped into caffeine-sensitive stores bearing impaired Ca^{2+} release machinery might be transferred into IP_3-sensitive stores retaining intact Ca^{2+} release assembly until it becomes overloaded in the mutant VSMCs. In addition to TRIC and Ca^{2+} release channels, many

Ca^{2+}-handling proteins are cooperatively functioning in the ER/SR at quite different levels among cell types. Recent live cell imaging revealed that the ER/SR membranes exhibiting cell-type specific ultrastructures are dynamic networks, constantly remodeling in a condition-dependent manner. Such protein-compositional, morphological and kinetic characteristics could underlie the Ca^{2+} laundering, as well as the preferential channel coupling discussed above. To evaluate these mysterious mechanisms proposed by *Tric-a*-knockout mice, VSMCs lacking or overexpressing TRIC-B channels would provide useful model systems in our future studies.

TRIC-A Variants Associated with Essential Hypertension

It is important to define lifestyle habits and genetic variations associated with hypertension, because it is a major risk factor for stroke and ischemic heart disease. Although genome-wide studies have recently identified several single nucleotide polymorphisms (SNPs) associated with susceptibility to essential hypertension in the human genome (for example, Newton-Cheh et al., 2009), the relationship between hypertension and the *TRIC-A* (*TMEM38A*) gene is unknown. To survey genetic mutations causative for hypertension in the *TRIC-A* gene, we sequenced genomic segments from Japanese patients with severe hypertension. Although no mutation was found in the analysis, we observed several common *TRIC-A* SNPs in linkage disequilibrium (LD) (Figure S7A). The HapMap database for genetic variants tentatively classified SNPs around the *TRIC-A* gene into three blocks; block 1 lying >30 kb upstream of the *TRIC-A* gene, block 2 located in the putative promoter overlapping with the neighboring gene and block 3 covering the *TRIC-A* transcriptional region (Figures 6A and S7B).

To examine the relationship between *TRIC-A* variants and hypertension, we conducted an association analysis of the tag SNPs selected from the LD blocks. In a Japanese population-based

case-control study using 1,119 hypertensive and 1,140 normotensive subjects (Table S1), PCR genotyping demonstrated that several LD SNPs in blocks 2 and 3 are positively associated with essential hypertension (Table 1). For example, in SNP rs901792 variations in block 3, the minor C allele with a frequency of ~30% was found to be a risk allele. The most significant association with hypertension was found at rs17796739, an LD SNP in block 2. All positively-associated SNPs in our analysis showed nearly absolute LD, i.e. LD=1 and high r^2, and blocks 2 and 3 formed a single LD block spanning the entire *TRIC-A* gene in the Japanese population. On the other hand, no significant association was found in non-LD SNPs in block 2 or 3, or in SNPs in block 1 (Figure 6 and Table 1).

TRIC-A Variants Associated with Efficacy of Antihypertensive Drugs

The "GEANE (Gene evaluation for antihypertensive effects of drugs) study" used ~130 Japanese hypertensive patients to examine the depressor effects of the angiotensin II AT1-receptor blocker valsartan (ARB), Ca^{2+} channel blocker amlodipine (CCB) and thiazide diuretic indapamide (TZD) at their standard doses (Table S2). When BP shifts were directly examined, microarray genotyping detected that these antihypertensive drugs are less effective for the hypertension risk allele homozygotes at LD SNP sites in the *TRIC-A* gene (Figure 6B and Table S3). For example, the patients with the CC genotype at rs901792 were low responders to the antihypertensive medications. When ARB-induced depressor effects were closely evaluated by adjusting for baseline BP values (Purcell et al., 2007), the CC-homozygous patients showed an insufficient diastolic BP (DBP) reduction compared to other genotypes, while no difference was detected in systolic BP (SBP) reduction between the genotypes (Figure 6C and Table S4). Therefore, the minor allele was associated with a DBP-resistant characteristic during ARB therapy. This significant association was

detected in four LD SNPs of blocks 2 and 3, but disappeared in SNPs of block 1.

Weak association of the hypertension-risk SNPs with insufficient DBP reduction was also observed in TZD and CCB therapies (Figure 6C). However, it is worth noting that the relationships of DBP-lowering effects with SNP genotypes were slightly different among the antihypertensive medications. For example, risk allele homozygotes at rs8112375 and rs10403969 were significantly associated with ARB resistance. Similar trends were observed in the CCB therapy, while no association was indicated in the TZD therapy. However, it is clear that additional studies in more patients are required to directly link the hypertension-risk SNPs to their different pharmacological efficacies between the antihypertensive medications.

TRIC-A Variants and *Tric-a*-Knockout Hypertension

The presented data demonstrated that the *TRIC-A* LD-SNPs are associated with essential hypertension and reduce the efficacy of antihypertensive agents. Therefore, these SNPs can contribute to developing preventive care approaches and personalized medication to treat hypertension. However, the biological alterations induced by the *TRIC-A* variants remain to be investigated in future studies. Based on our data from *Tric-a*-knockout mice, it may be reasonably assumed that the *TRIC-A* minor allele as a hypertension risk is accompanied by weak gene expression in VSMCs. Indeed, the block 2 SNPs at the putative promoter region showed slightly lower *p* values in association with hypertension than the block 3 SNPs (Table 1). In this regard, there may be a discrepancy between observations from *Tric-a*-knockout mice and hypertensive patients, i.e. *Tric-a*-knockout mice were hypersensitive to Ca^{2+} channel antagonists (Figure 1), but amlodipine exerted poor depressor effects in hypertensive patients homozygous for the *TRIC-A* risk allele (Figure 6). However, the Ca^{2+} channel antagonists were administered at submaximal doses to

the knockout mice, while amlodipine was dispensed at a regular dose within the safety margin to the hypertensive patients. The knockout mice bearing apparently uniform genetic backgrounds develop monogenic hypertension, while combined multigenic factors and lifestyle habits including aging effects give rise to essential hypertension in human subjects with non-uniform genetic backgrounds. Therefore, appropriate care must be taken when directly comparing of the data from the knockout mice and hypertensive patients.

Our finding with *Tric-a*-knockout mice redefined aspects of the contribution of SR Ca^{2+}-handling in VSMCs to physiological BP maintenance. As in the case of TRIC-A channels, BK channels contribute to hyperpolarization signaling in VSMCs, and several variants of the BK channel subunit genes are highly associated with hypertension (Köhler, 2010). As well as the *TRIC-A* gene, our present observations may implicate the genes encoding other SR Ca^{2+}-handling proteins as candidates for genes that contribute to pathology in essential hypertension.

EXPERIMENTAL PROCEDURES

Hemodynamic and Myogenic Tone Measurements

Tric-a-knockout mice were generated as described previously (Yazawa et al., 2007), and all experiments were predominantly designed using young-adult male mice (8−12 weeks old) in this study. For SMC-specific expression of TRIC-A channels, a transgene was constructed by inserting the mouse *Tric-a* cDNA between the α-smooth muscle actin promoter and the polyadenylation sequence (Nakano et al., 1991). Circadian hemodynamic profiles were analyzed using implantable devices in telemetric BP and electrocardiogram monitoring systems (Data Sciences International, USA.). BP and HR were also monitored by conventional tail-cuff plethysmography (Softron, Japan).

Myogenic tone and isometric tension measurements in vascular preparations were carried out as described previously (Iwamoto et al., 2004).

Physiological Measurements in VSMCs

The vessel preparations were used for anatomical and gene expression analyses (Yazawa et al, 2007; Hotta et al., 2007). To examine Ca^{2+} handling in VSMCs, endothelial cells were removed from vascular preparations, and the resulting segments were incubated with Fura-PE3AM and subjected to ratiometric imaging with excitation at 340 and 380 nm, and emission at >510 nm (Iwamoto et al., 2004). Cultured endothelial cells from the aorta were subjected to immunocytochemistry and Fura-2 Ca^{2+} imaging (Kobayashi et al., 2005).

To monitor Ca^{2+} sparks, single VSMCs prepared from mesenteric arteries (Ohi et al., 2001) were incubated with Fluo-4AM, and subjected to imaging with excitation at 488 nm and emission at >520 nm using a total internal reflection fluorescence microscopy system. To monitor Mn^{2+} quench of Fura-2 fluorescence, VSMCs loaded with Fura-2AM were subjected to imaging with excitation at 360 nm and emission at >510 nm (Hashii et al., 2000). To measure K^+ and Ca^{2+} channel currents, the whole-cell voltage clamp technique was applied to isolated VSMCs (Hotta et al., 2007; Ohi et al., 2001). Although widely used voltage-sensitive dyes often activate BK channels, such side effects of oxonol VI seem to be minimal (Morimoto et al., 2007). To monitor membrane potential using oxonol VI (Apell and Bersch, 1987), isolated VSMCs were subjected to confocal-microscopic imaging with excitation at 559 nm and emission at >606 nm (Masumiya et al., 2009).

Case-Control and GEANE Studies

Hypertensive cases and normotensive controls were recruited from several regions in Japan.

Genomic DNAs from blood samples were genotyped with the TaqMan probe assay using primers and probes purchased from the Assay-on-Demand system (Applied Biosystems). Frequency differences in each SNP were assessed by the chi-square test. The GEANE study utilized an open random crossover protocol to examine the antihypertensive effects of ARB, TZD and CCB in untreated Japanese with essential hypertension. Before and after each drug medication for three months, BP was determined and blood samples were collected for SNP genotyping (Human Mapping 500K, Affymetrix). The data were examined in the two evaluation models (Purcell et al., 2007): (i) linear regression for differences in BP from pre-medication to post-medication with only SNPs as a fixed effect (Figure 6B) and (ii) linear regression for post-medication BP with SNPs and pre-medication BP as covariates (Figure 6C).

SUPPLEMENTAL INFORMATION

Supplemental Information includes seven figures, five tables and experimental procedures can be found with this article online at xx.

ACKNOWLEDGEMENTS

We thank Miss. Yuki Mizobe and Masako Nishida for technical assistance, Drs Takeru Makiyama and and Hitoshi Okamura for support in HR and BP monitoring, Dr. Takeshi Miwa for providing the SMC-specific promoter, Drs Noah Weisleder and Jianjie Ma for valuable comments, and Drs Katsuhiko Kohara, Ryuichi Kawamoto, Tomohiro Katsuya, Tomohiro Nakayama and Nobuhito Hirawa for support in the case-control study. This work was supported in part by grants from the

Ministry of Education, Culture, Sports, Science and Technology, the Ministry of Health and Welfare, the US National Institute of Health, the Takeda Science Foundation, the Astellas Foundation, the Mochida Memorial Foundation, the Kanae Foundation, the Daiichi-Sankyo Foundation of Life Science, the Salt Science Research Foundation, the Japan Health Foundation for the Prevention of Chronic Diseases and the Improvement of QOL of Patients, the Sakakibara Memorial Research Foundation, the Yokoyama Foundation, the UBE Foundation and the Vehicle Racing Commemorative Foundation.

REFERENCES

Amberg, G.C., Navedo, M.F., Nieves-Cintrón, M., Molkentin, J.D., and Santana, L.F. (2007). Calcium sparklets regulate local and global calcium in murine arterial smooth muscle. J. Physiol. *579*, 187–201.

Apell, H.J., and Bersch, B. (1987). Oxonol VI as an optical indicator for membrane potentials in lipid vesicles. Biochim. Biophys. Acta. *903*, 480–494.

Berridge, M.J. (2008). Smooth muscle cell calcium activation mechanisms. J. Physiol. *586*, 5047–5061.

Busse, R., Edwards, G., Félétou, M., Fleming, I., Vanhoutte, P.M., and Weston, A.H. (2002). EDHF: bringing the concepts together. Trends Pharmacol. Sci. *23*, 374–380.

Cheng, H., and Lederer, W.J. (2008). Calcium sparks. Physiol. Rev. *88*, 1491–1545.

Fleischer, S. (2008). Personal recollections on the discovery of the ryanodine receptors of muscle. Biochem. Biophys. Res. Commun. *369*, 195–207.

Hashii, M., Minabe, Y., and Higashida, H. (2000). cADP-ribose potentiates cytosolic Ca^{2+} elevation and Ca^{2+} entry via L-type voltage-activated Ca^{2+} channels in NG108-15 neuronal cells. Biochem. J.

345, 207–215.

Hotta, S., Morimura, K., Ohya, S., Muraki, K., Takeshima, H., and Imaizumi, Y. (2007). Ryanodine receptor type 2 deficiency changes excitation-contraction coupling and membrane potential in urinary bladder smooth muscle. J. Physiol. *582*, 489–506.

Iino, M. (1990). Biphasic Ca^{2+} dependence of inositol 1,4,5-trisphosphate-induced Ca release in smooth muscle cells of the guinea pig taenia caeci. J. Gen. Physiol. *95*, 1103–1122.

Iwamoto, T., Kita, S., Zhang, J., Blaustein, M.P., Arai, Y., Yoshida, S., Wakimoto, K., Komuro, I., and Katsuragi, T. (2004). Salt-sensitive hypertension is triggered by Ca^{2+} entry via Na^{+}/Ca^{2+} exchanger type-1 in vascular smooth muscle. Nat. Med. *10*, 1193–1199.

Kobayashi, M., Inoue, K., Warabi, E., Minami, T., and Kodama, T. (2005). A simple method of isolating mouse aortic endothelial cells. J. Atheroscler. Thromb. *12*, 138–142.

Kockskämper, J., Zima, A.V., Roderick, H.L., Pieske, B., Blatter, L.A., and Bootman, M.D. (2008). Emerging roles of inositol 1,4,5-trisphosphate signaling in cardiac myocytes. J. Mol. Cell. Cardiol. *45*, 128–147.

Koshita, M., Hidaka, K., Ueno, H., Yamamoto, Y., and Suzuki, H. (2007). Properties of acetylcholine-induced hyperpolarization in smooth muscle cells of the mouse mesenteric artery. J. Smooth Muscle Res. *43*, 219–227.

Köhler, R. (2010). Single-nucleotide polymorphisms in vascular Ca^{2+}-activated K^{+}-channel genes and cardiovascular disease. Pflugers Arch. *460*, 343–351.

Masumiya, H., Asaumi, Y., Nishi, M., Minamisawa, S., Adachi-Akahane, S., Yoshida, M., Kangawa, K., Ito, K., Kagaya, Y., Yanagisawa, T., et al. (2009). Mitsugumin 53-mediated maintenance of K^{+} currents in cardiac myocytes. Channels *3*, 6−11.

Meissner, G. (1983). Monovalent ion and calcium ion fluxes in sarcoplasmic reticulum. Mol. Cell. Biochem. *55*, 65–82.

Morimoto, T., Sakamoto, K., Sade, H., Ohya, S., Muraki, K., and Imaizumi, Y. (2007).

Voltage-sensitive oxonol dyes are novel large-conductance Ca^{2+}-activated K^+ channel activators selective for beta1 and beta4 but not for beta2 subunits. Mol. Pharmacol. *71*, 1075–1088.

Nakano, Y., Nishihara, T., Sasayama, S., Miwa, T., Kamada, S., and Kakunaga, T. (1991). Transcriptional regulatory elements in the 5' upstream and first intron regions of the human smooth muscle (aortic type) α-actin-encoding gene. Gene *99*, 285–289.

Nelson, M.T., Cheng, H., Rubart, M., Santana, L.F., Bonev, A.D., Knot, H.J., and Lederer, W.J. (1995). Relaxation of arterial smooth muscle by calcium sparks. Science *270*, 633–637.

Newton-Cheh, C., Johnson, T., Gateva, V., Tobin, M.D., Bochud, M., Coin, L., Najjar, S.S., Zhao, J.H., Heath, S.C., Eyheramendy, S., et al. (2009). Genome-wide association study identifies eight loci associated with blood pressure. Nat. Genet. *41*, 666–676.

Ohi, Y., Yamamura, H., Nagano, N., Ohya, S., Muraki, K., Watanabe, M., and Imaizumi, Y. (2001). Local Ca^{2+} transients and distribution of BK channels and ryanodine receptors in smooth muscle cells of guinea-pig vas deferens and urinary bladder. J. Physiol. *534*, 313–326.

Patterson, R.L., Boehning, D., and Snyder, S.H. (2004). Inositol 1,4,5-trisphosphate receptors as signal integrators. Annu. Rev. Biochem. *73*, 437–465.

Pitt, S.J., Park, K.H., Nishi, M., Urashima, T., Aoki, S., Yamazaki, D., Ma, J., Takeshima, H., and Sitsapesan, R. (2010). Charade of the SR K^+-channel: two ion-channels, TRIC-A and TRIC-B, masquerade as a single K^+-channel. Biophys. J. *99*, 417–426.

Purcell, S., Neale, B., Todd-Brown, K., Thomas, L., Ferreira, M.A., Bender, D., Maller, J., Sklar, P., de Bakker, P.I., Daly, M.J., et al. (2007). PLINK: a tool set for whole-genome association and population-based linkage analyses. Am. J. Hum. Genet. *81*, 559–575.

Segal, S.S. (1994). Cell-to-cell communication coordinates blood flow control. Hypertension *23*, 1113–1120.

Smyth, J.T., Dehaven, W.I., Jones, B.F., Mercer, J.C., Trebak, M., Vazquez, G., and Putney, J.W. Jr. (2006). Emerging perspectives in store-operated Ca^{2+} entry: roles of Orai, Stim and TRP. Biochim. Biophys. Acta. *1763*, 1147–1160.

Wei, A.D., Gutman, G.A., Aldrich, R., Chandy, K.G., Grissmer, S., and Wulff, H. (2005). International Union of Pharmacology. LII. Nomenclature and molecular relationships of calcium-activated potassium channels. Pharmacol. Rev. *57*, 463–472.

Wellman, G.C., and Nelson, M.T. (2003). Signaling between SR and plasmalemma in smooth muscle: sparks and the activation of Ca^{2+}-sensitive ion channels. Cell Calcium *34*, 211–229.

Wray, S., and Burdyga, T. (2010). Sarcoplasmic reticulum function in smooth muscle. Physiol. Rev. *90*, 113–178.

Yamazaki, D., Komazaki, S., Nakanishi, H., Mishima, A., Nishi, M., Yazawa, M., Yamazaki, T., Taguchi, R., and Takeshima, H. (2009). Essential role of the TRIC-B channel in Ca^{2+} handling of alveolar epithelial cells and in perinatal lung maturation. Development *136*, 2355–2361.

Yazawa, M., Ferrante, C., Feng, J., Mio, K., Ogura, T., Zhang, M., Lin, P.H., Pan, Z., Komazaki, S., Kato, K., et al. (2007). TRIC channels are essential for Ca^{2+} handling in intracellular stores. Nature *448*, 78–82.

Zhao, X., Yamazaki, D., Park, K.H., Komazaki, S., Tjondrokoesoemo, A., Nishi, M., Lin, P., Hirata, Y., Brotto, M., Takeshima, H., et al. (2010). Ca^{2+} overload and sarcoplasmic reticulum instability in tric-a null skeletal muscle. J. Biol. Chem. *285*, 37370–37376.

Table 1. Association of *TRIC-A* Tag SNPs with Essential Hypertension

		genotype frequency (*n*)		association analysis		Linkage disequilibrium			
		hypertensive	normotensive	odds (95% CI)	*p*	block	D'	LOD	r^2
rs2363857	GG/GA/AA	1/40/1089	1/46/1065	0.86 (0.57−1.30)	0.47	block 1	0.826	3.72	0.004
rs1020723	GG/GA/AA	3/73/1052	0/79/1032	0.98 (0.72−1.35)	0.92	block 1	0.586	2.00	0.004
rs17796739	TT/TC/CC	75/390/624	54/378/683	1.18 (1.03−1.36)	0.018*	block 2		reference	
rs2279448	CC/CT/TT	3/116/972	5/112/1006	1.03 (0.80−1.33)	0.816	block 2	1.000	13.98	0.018
rs8101030	AA/AC/CC	92/437/576	75/416/634	1.16 (1.02−1.33)	0.026*	block 2	0.995	617.54	0.843
rs4808521	GG/GA/AA	97/455/555	87/428/614	1.14 (1.00−1.30)	0.048*	block 3	0.913	436.24	0.666
rs730120	AA/AG/GG	69/397/641	55/380/699	1.16 (1.01−1.33)	0.041*	block 3	0.973	658.63	0.911
rs901792	CC/CT/TT	114/481/496	108/444/558	1.14 (1.00−1.29)	0.048*	block 3	0.928	384.36	0.587
rs2431808	GG/GA/AA	9/170/952	11/167/928	1.03 (0.84−1.27)	0.779	block 3	0.185	0.52	0.001
rs2279449	AA/AG/GG	26/247/829	31/276/824	0.89 (0.76−1.06)	0.189	block 3	0.984	35.20	0.048

The case and control subjects were genotyped, and the data were analyzed using an allelic model. Statistical differences between the genotypes are indicated by an asterisk (*p<0.05). CI, confidence interval. The tag SNPs examined were selected from the 110-kb region (chromosome 19, 16560K to 16670K in the HapMap database), in which three LD blocks were proposed in the analysis using Haploview software (see Figure S7). Pairwise LD properties were calculated using rs17796739 as a reference; the standardized disequilibrium coefficient (D'), logarithm of odds (LOD) and squared allele-frequency correlation (r^2) are given.

Figure legends

Figure 1. Hypertensive and Bradycardiac Phenotypes in *Tric-a*-Knockout Mice

(**A** and **B**) Daytime hypertension and bradycardia in *Tric-a*-knockout mice. Circadian fluctuations in systolic BP (**A**) and HR (**B**) were telemetrically monitored, and the data were averaged over each 2-hr interval during a 24 hr period. (**C**) BP and HR monitoring by tail-cuff plethysmography during daytime. Autonomic controls were blocked by intraperitoneal injections of the muscarinic antagonist atropine (Atr, 4 mg/kg) and β1-antagonist metoprolol (Met, 4 mg/kg). (**D**) BP-lowering effects of depressors at submaximal doses. Drugs injected intraperitoneally were Pra (α1-antagonist prazosin, 1 mg/kg), Clo (α2-agonist clonidine, 0.1 mg/kg), Can (angiotensin II AT1-receptor blocker candesartan, 10 mg/kg), BQ123 (endothelin A-receptor blocker, 1 mg/kg), OPC (vasopressin V1-receptror blocker OPC-21268, 10 mg/kg), Y27632 (Rho kinase inhibitor, 5 mg/kg), Nic (dihydropyridine Ca^{2+} antagonist nicardipine, 1 mg/kg), Ver (phenylalkylamine Ca^{2+} antagonist verapamil, 12 mg/kg), HOE (bradykinin antagonist HOE140, 1 mg/kg), and hAM (adrenomedullin antagonist hAM22–52, 20 mg/kg). The data represent the mean ± SEM., and the numbers of mice examined are shown in parentheses. Statistical differences between the genotypes are indicated by asterisks (*p<0.05, **p<0.01 in t-test).

Figure 2. Enhanced Tonus in *Tric-a*-Knockout Arteries and Abnormal Ca^{2+}-Handling in *Tric-a*-Knockout VSMCs

(**A**–**C**) Myogenic tone measurements in mesenteric arteries. Representative recording data are shown in **A**. The dotted line indicates the passive diameter (PD) determined in a Ca^{2+}-free solution. Myogenic tone (MT) is expressed as the difference between the steady-state and passive diameters at an intravascular pressure of 70 mmHg. The data for the pressure-diameter relationship and MT are summarized in **B** and **C**, respectively. (**D**–**M**) Ca^{2+}

imaging in arterial VSMC segments. Representative effects of extracellular Ca^{2+} and L-type Ca^{2+} channel modulators on resting $[Ca^{2+}]i$ are shown in **D**, and the data are summarized in **E**. L-type Ca^{2+} channels were activated or inhibited by BayK8644 or verapamil, respectively. Representative SR Ca^{2+} leakage and store-operated Ca^{2+} entry responses (SOCE) are shown in **F**, and the data are summarized in **G**. Ca^{2+} leakage induced by the Ca^{2+}-pump inhibitor cyclopiazonic acid (CPA) reflects total SR Ca^{2+} content. Representative Ca^{2+} transients induced by caffeine (Caf) are shown in **H**, and the data are summarized in **I**. Because caffeine activates RyRs, the Ca^{2+} transient represents the Ca^{2+} content of stores bearing RyRs. Representative agonist-induced Ca^{2+} transients are shown in **J**, and the data are summarized in **K**. Because the α1-agonist phenylephrine (PE) induces IP_3R-mediated Ca^{2+} release, the Ca^{2+} transient reflects the Ca^{2+} content of stores bearing IP_3Rs. Sequential responses upon PE and Caf under Ca^{2+}-free conditions are shown in **L**, and the data are summarized in **M**. The data represent the mean ± SEM., and the numbers of mice examined are shown in parentheses. Statistical differences between the genotypes are indicated by asterisks (*p<0.05, **p<0.01 in ANOVA or t-test). Statistically significant drug-induced effects within each genotype are indicated by sharps (#p<0.05, ##p<0.01 in t-test).

Figure 3. Impaired Hyperpolarization Signaling in *Tric-a*-Knockout VSMCs

(**A**–**D**) Ca^{2+} spark imaging. Single VSMCs were prepared from mesenteric arteries and loaded with Fluo-4 for total internal reflection fluorescence imaging. Ca^{2+} sparks were monitored in normal (5.9 mM KCl) and high-K^+ (60 mM KCl) bathing solutions. Representative data from the high-K^+ measurements are shown in **A**. Ca^{2+} sparks generated at the numbered time points are shown as pseudocolor-coded images in upper panels. The intracellular fluorescence intensity was normalized to the baseline intensity to yield the relative intensity (F/F_0), and time courses of the intensity

changes at the subcellular regions (see colored circles in the upper left images, scale bar = 10 μm) are illustrated in the lower traces. The data on spark frequency (**B**), spark amplitude (**C**) and spark spot number (**D**) are summarized. (**E**–**G**) STOC measurements. The membrane potential of isolated VSMCs was controlled by the whole-cell patch-clamp technique to monitor membrane currents. Representative recording data are shown in **E**. The data of STOC frequency (**F**) and amplitude (**G**) are summarized. The data represent the mean ± SEM., and the numbers of cells examined from at least 3 mice are shown in parentheses. Statistical differences between the genotypes are indicated by asterisks (*p<0.05, **p<0.01 in t-test).

Figure 4. Enhanced Excitability in *Tric-a*-Knockout VSMCs

In single VSMCs perfused with the bathing solution containing oxonol VI, cellular fluorescence intensities were monitored by confocal-microscopic imaging and normalized to the maximum value in the 140 mM KCl solution to yield the fractional intensity (F/F_{140K}). Representative recoding data are shown in **A**. The data of the resting intensity are summarized in **B**. To prepare a calibration plot, the data from bathing solutions containing 5.9 (normal solution), 20, 30, 60 and 140 mM KCl, together with the reported value of resting membrane potential, are summarized in **C**; red and blue lines indicate the resting fractional intensity and estimated resting membrane potential of VSMCs prepared from the knockout and rescue mice, respectively. The data of the intensity shift by iberiotoxin (IBTX) are summarized in **D**. The decay time courses of the fluorescence intensity after replacing the 60 mM KCl bathing solution with the normal solution are shown in **E**; fluorescence intensities were normalized to the value in the 60 mM KCl solution. The half-decay time was significantly prolonged in *Tric-a*-knockout VSMCs under normal conditions, but no difference between the genotypes was observed in the presence of IBTX (**F**). The data represent the mean ±

SEM., and the numbers of cells examined from at least 3 mice are shown in parentheses. Statistical differences between the genotypes are indicated by asterisks (*p<0.05, **p<0.01 in t-test).

Figure 5. Compromised Ca^{2+} signaling in *Tric-a*-Knockout VSMCs

The loss of TRIC-A channels seems directly to inhibit Ca^{2+} spark generation mediated by RyRs, thus attenuating the hyperpolarization signaling produced by functional coupling between RyRs and BK channels and elevating resting membrane potential in VSMCs. In the situation, L-type Ca^{2+} channels (Cav) are hyperactivated and resting $[Ca^{2+}]i$ are elevated to develop enhanced spontaneous tonus in resistance arteries and hypertension in the knockout mice. Upon sympathetic stimulation, the α1-adrenoceptor (α1AR), trimeric GTP-binding protein Gq, and phospholipase C (PLC) are coordinately activated to trigger IP_3R-mediated Ca^{2+} release. In *Tric-a*-knockout VSMCs, poor Ca^{2+} sparks may conversely develop SR Ca^{2+} overloading to boost IP_3R-mediated Ca^{2+} release as the contraction signaling.

Figure 6. *TRIC-A* SNPs Associated with Hypertension and Antihypertensive Efficacy

(**A**) LD plot of genomic region encompassing *TRIC-A* gene. The plot was illustrated with common SNPs and downloaded from the HapMap database. The *C19ORF42* gene encodes a hypothetical protein. The transcriptional direction of each gene is indicated by an arrow. LD SNPs around the *TRIC-A* gene cluster to generate the blocks 1–3 (block 1 is located outside of this map, see Figure S7B). Of SNPs genotyped in the case-control study (red rs ID), five SNPs showing significant association with hypertension (see Table 1) were in tight LD. Of eight SNPs examined in the GEANE study, five sites are localized in blocks 2 and 3 (blue rs ID), but three sites are in the 3'-flanking region outside of the map region. Two SNPs were examined in both the case-control

and GEANE studies (purple rs ID). (**B** and **C**) In the GEANE study, valsartan (ARB), indapamide (TZD) and amlodipine (CCB) were administered at standard doses to hypertensive patients, and association of SNP genotypes with the hypotensive effects was examined. (**B**) When drug-induced reductions in mean BP (ΔMBP) were compared among SNP genotypes, insufficient BP-lowering effects were found to be associated with minor allele homozygosity at *TRIC-A* LD-SNPs including rs901792. The data represent the mean ± SD., and the subject numbers are shown in parentheses. **p*<0.05, ***p*<0.01 in *t*-test. (**C**) To further analyze the BP-lowering effects, SBP and DBP data were subjected to a regression analysis adjusting for baseline values before drug administration. In the bar graphs, the β values represent specific drug-induced effects in the minor allele homozygotes. The filled circles indicate *p* values (red circles, *p*<0.05 in *t*-test) at each SNP site. See Tables S3 and S4 for the overall picture of the analysis.

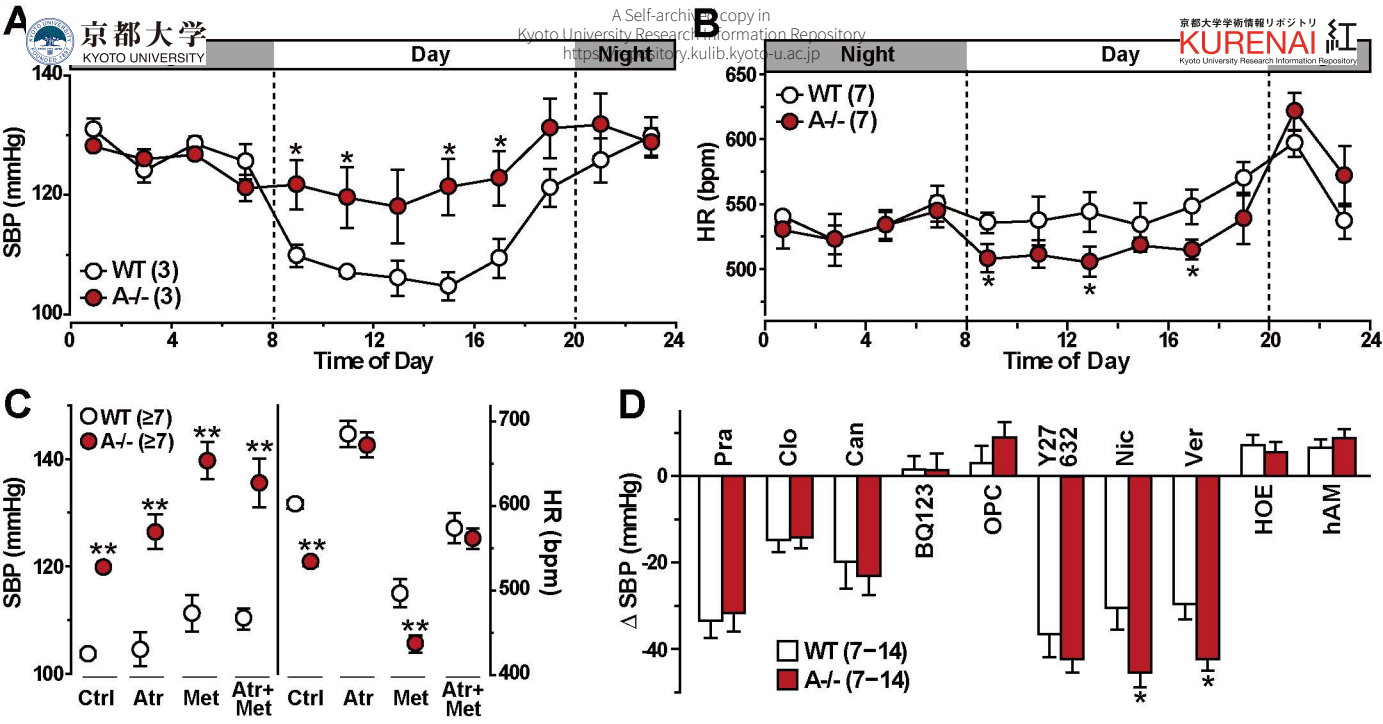

Figure 1

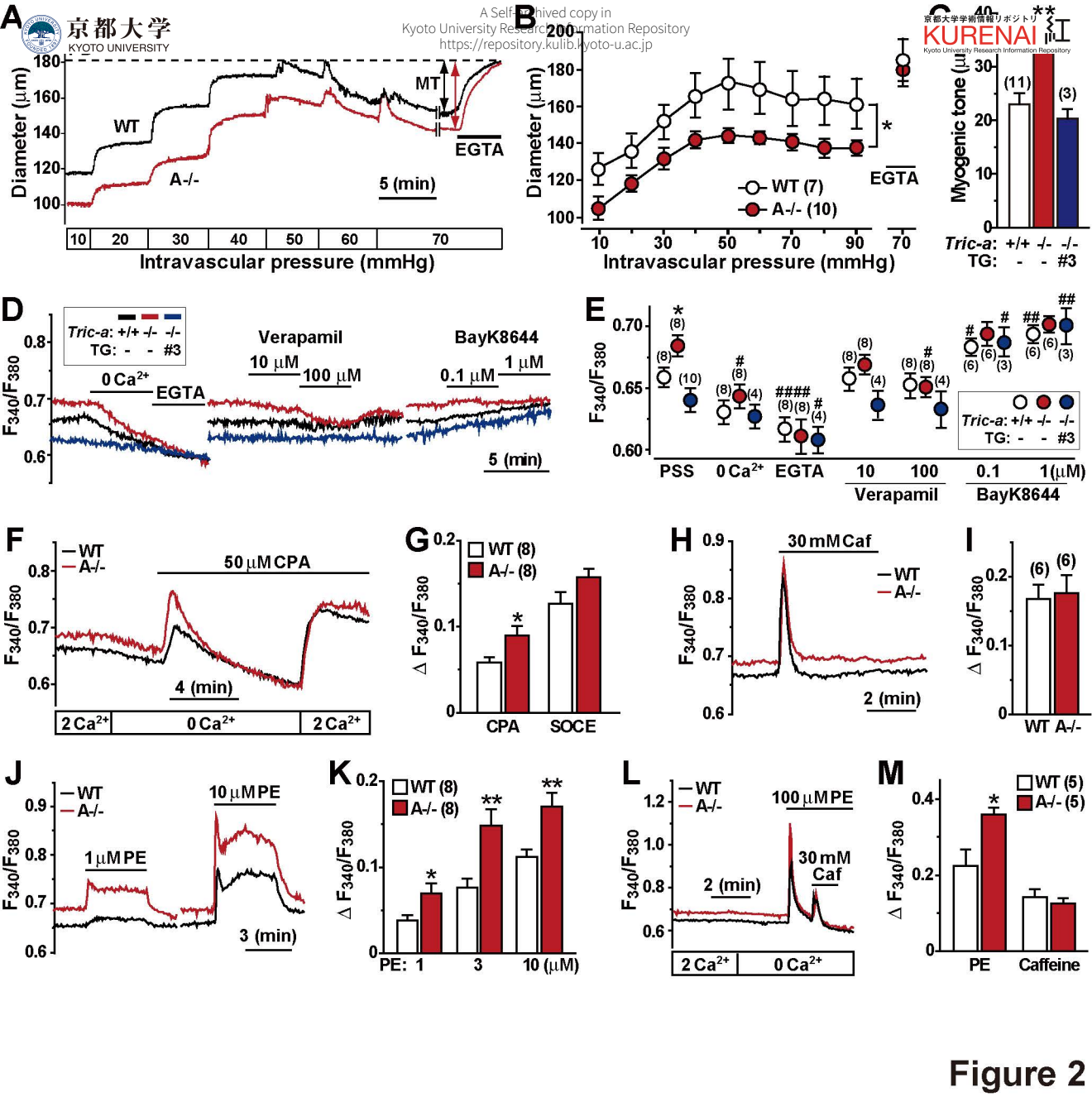

Figure 2

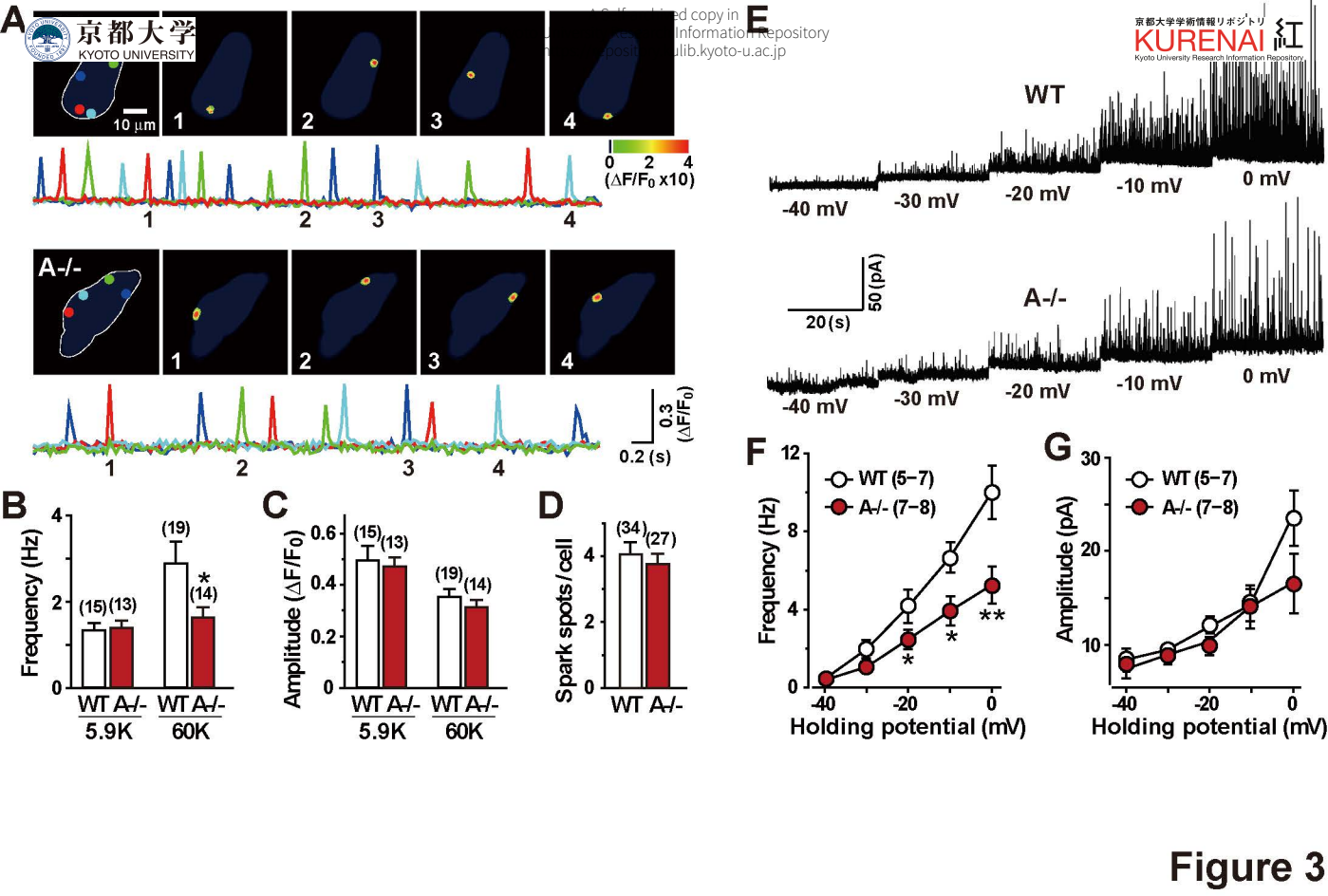

Figure 3

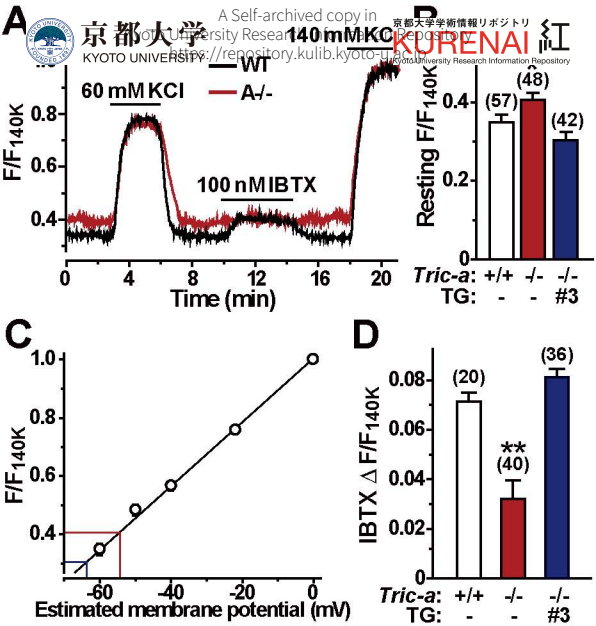

Figure 4

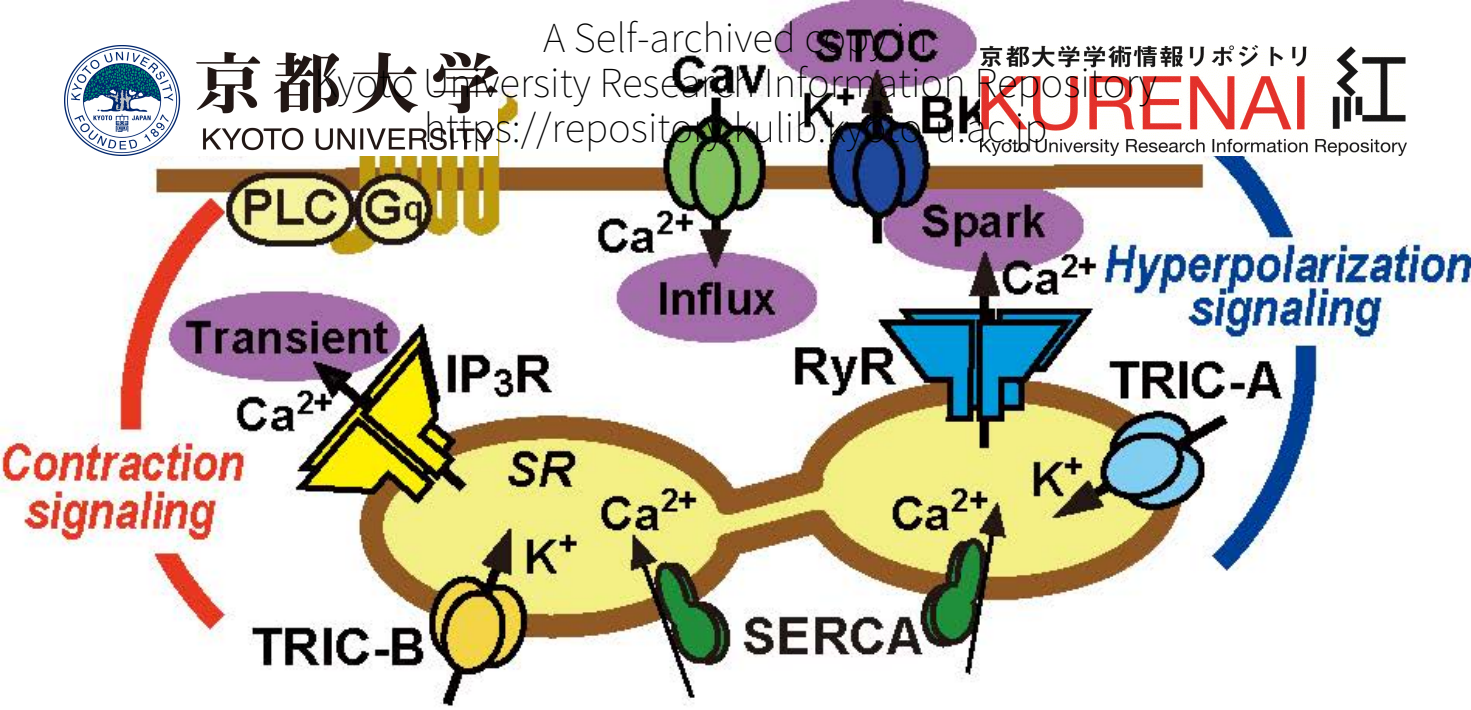

Wild-type VSMCs

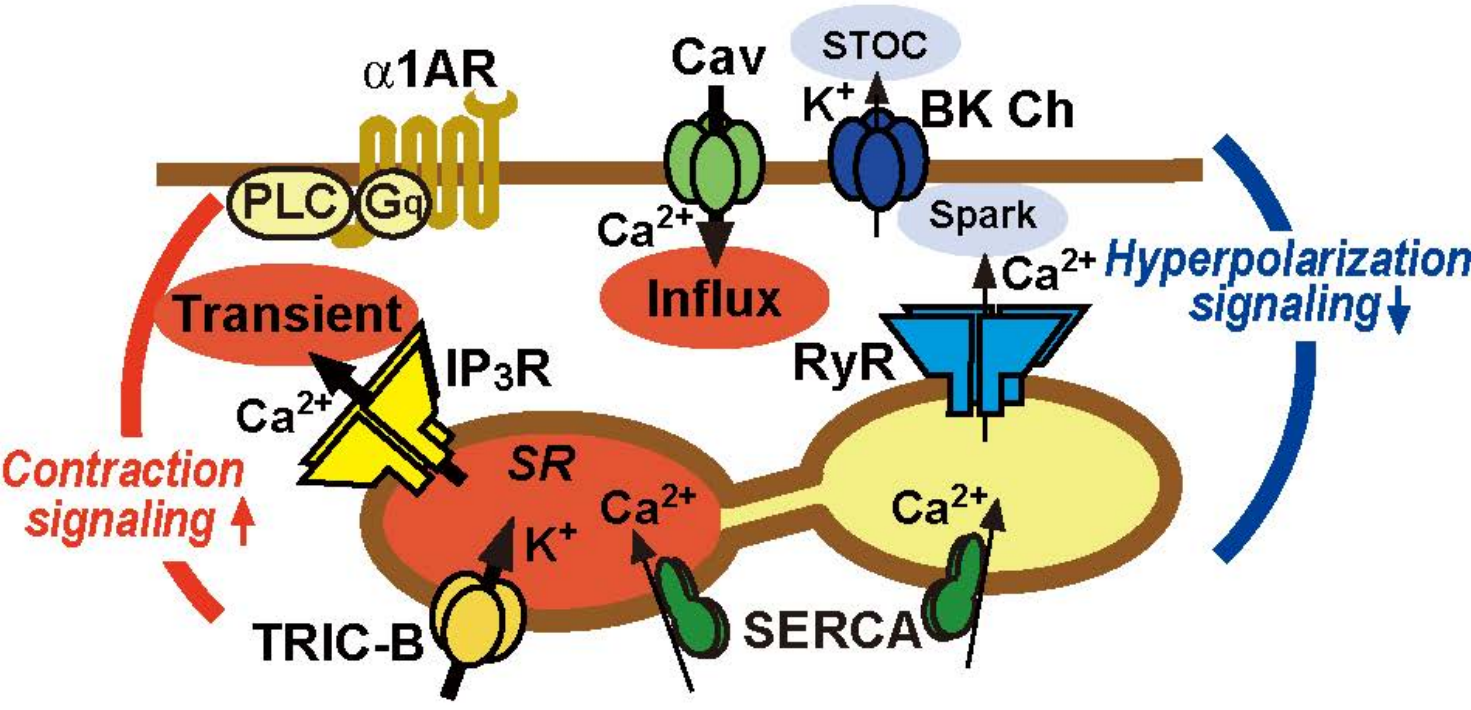

Tric-a-knockout VSMCs

Figure 5

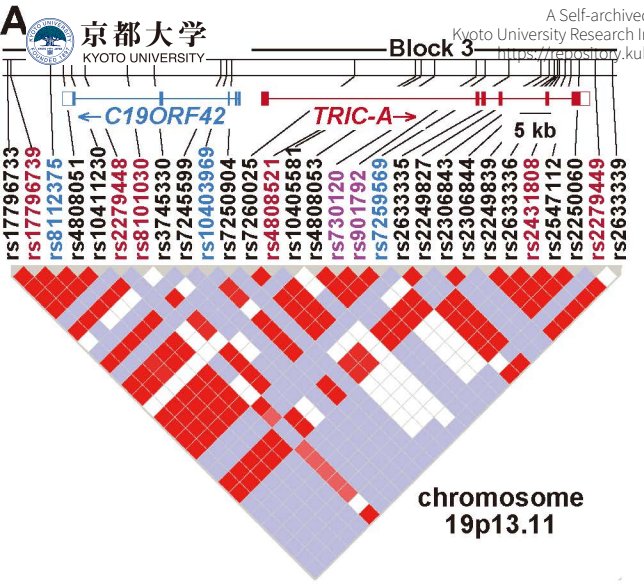

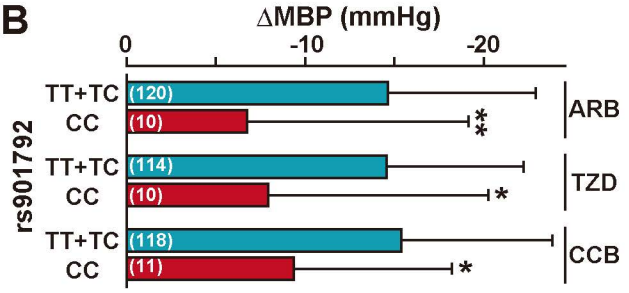

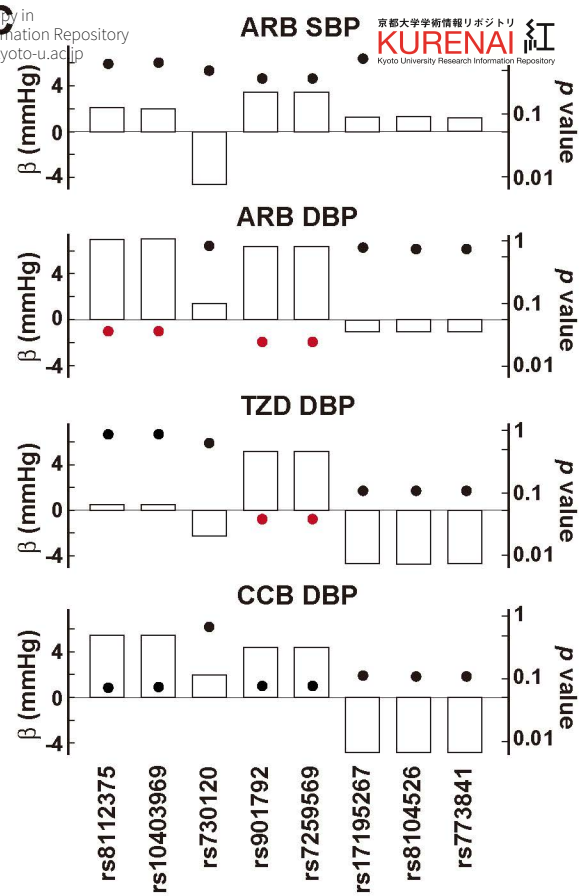

Figure 6

Cell Metabolism

Supplemental Information

TRIC-A Channels in Vascular Smooth Muscle Contribute to Blood Pressure Maintenance

Daiju Yamazaki, Yasuharu Tabara, Satomi Kita, Hironori Hanada, Shinji Komazaki, Daisuke Naitou, Aya Mishima, Miyuki Nishi, Hisao Yamamura, Shinichiro Yamamoto, Sho Kakizawa, Hitoshi Miyachi, Shintaro Yamamoto, Toshiyuki Miyata, Yuhei Kawano, Kei Kamide, Toshio Ogihara, Akira Hata, Satoshi Umemura, Masayoshi Soma, Norio Takahashi, Yuji Imaizumi, Tetsuro Miki, Takahiro Iwamoto, and Hiroshi Takeshima

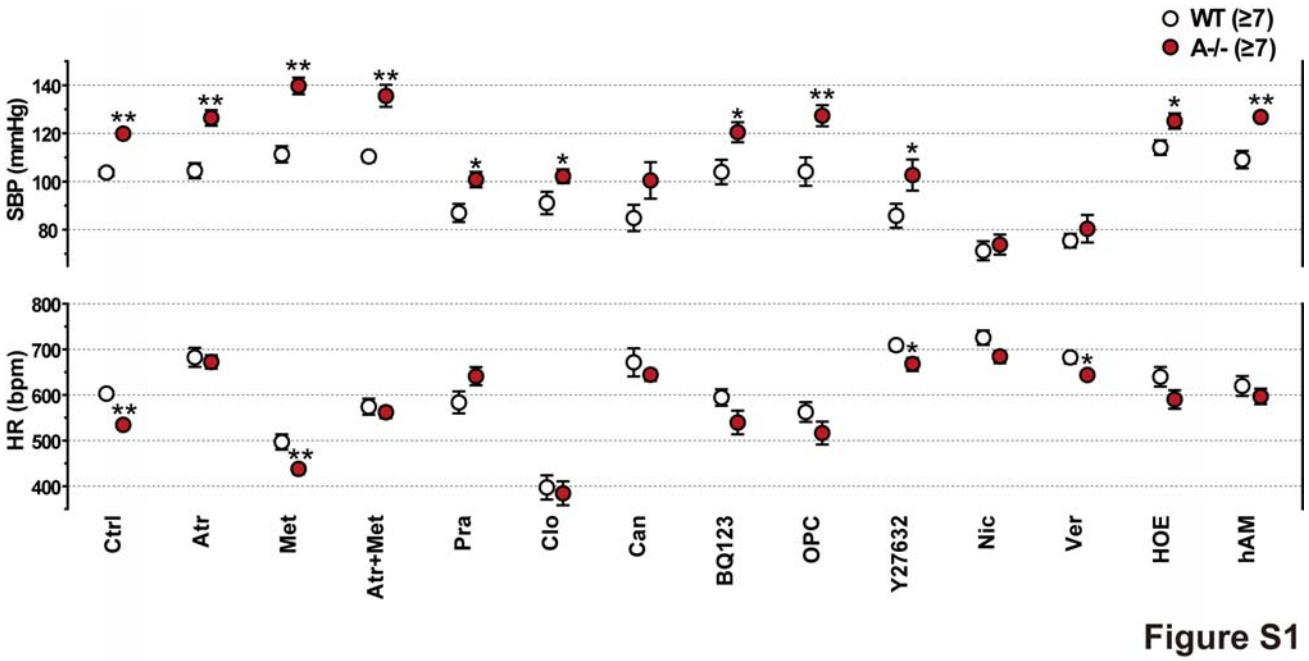

Figure S1. Effects of Hypotensive Agents on BP and HR in *Tric-a*-Knockout Mice

Pharmacological effects of various agents on systolic BP and HR were monitored by tail-cuff plethysmography in *Tric-a*-knockout and wild-type mice during daylight hours. Drugs used for the analysis are the muscarinic antagonist atropine (Atr, 4 mg/kg), β1-antagonist metoprolol (Met, 4 mg/kg), α1-antagonist prazosin (Pra, 1 mg/kg), α2-agonist clonidine (Clo, 0.1 mg/kg), angiotensin II AT1-receptor blocker candesartan (Can, 10 mg/kg), endothelin A-receptor blocker BQ123 (1 mg/kg), vasopressin V1-receptor blocker OPC-21268 (OPC, 10 mg/kg), Rho kinase inhibitor Y27632 (5 mg/kg), dihydropyridine Ca^{2+} antagonist nicardipine (Nic, 1 mg/kg), phenylalkylamine Ca^{2+} antagonist verapamil (Ver, 12 mg/kg), bradykinin antagonist HOE140 (HOE, 1 mg/kg) and adrenomedullin antagonist hAM22−52 (hAM, 20 mg/kg). The data represent the mean ± SEM., and the numbers of mice examined are shown in parentheses. Statistical differences between the genotypes are indicated by asterisks (*p<0.05, **p<0.01 in t-test).

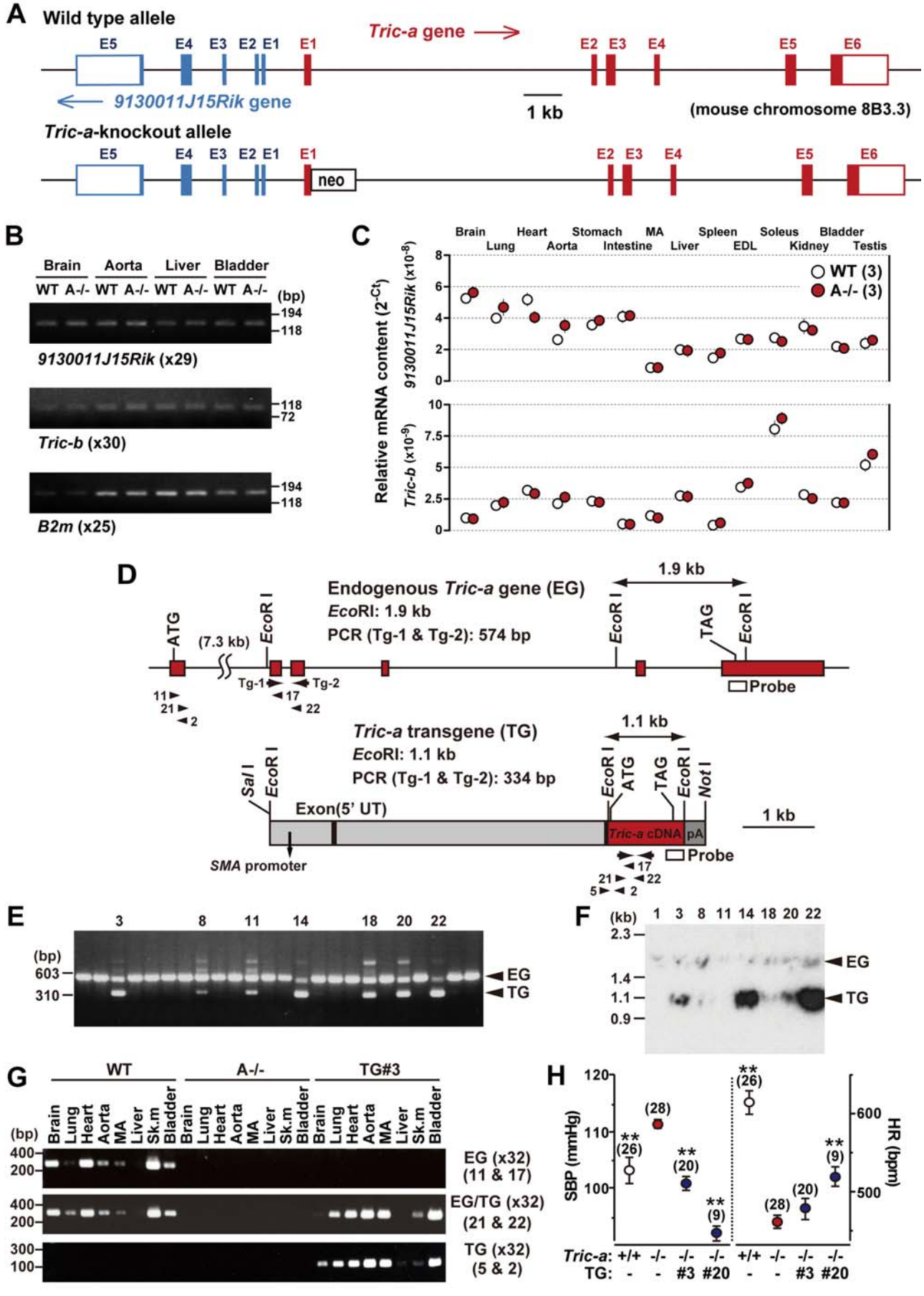

Figure S2

Figure S2. No Contribution of *9130011J15Rik* Gene to *Tric-a*-Knockout Hypertension

(**A**) Mouse genetic maps of wild-type and *Tric-a*-knockout alleles. The *Tric-a* gene (red) and the hypothetical gene (blue) are located close on chromosome 8B3.3. This proximity is probably shared by other mammalian genomes (see Figure 6 for the human genome). The putative genes encode hypothetical proteins, 9130011J15Rik in mouse and C19ORF42 in human, both of which are composed of 75 highly conserved amino acid residues. E1−E6 indicate exons in the genes; filled and open boxes represent protein-coding and noncoding regions, respectively. In the mutant allele, the neomycin resistance gene (neo) is ectopically inserted into the exon 1 of the *Tric-a* gene. (**B**) Quantitative detection of *9130011J15Rik* and *Tric-b* mRNAs in mouse tissues. Total tissue RNA preparations from at least 3 mice in each genotype were examined by quantitative RT-PCR. Amplified cDNAs were subjected to agarose gel electrophoresis, and representative data for cDNA amplification are presented. PCR cycle numbers are shown in parentheses, and β2-microglobulin (*B2m*) mRNA was examined as an internal control. (**C**) Relative contents of *9130011J15Rik* and *Tric-b* mRNAs in mouse tissues. MA, mesenteric artery; EDL, extensor digitorum longus muscle. The quantitative RT-PCR experiments detected no significant difference in *9130011J15Rik* or *Tric-b* mRNA expression between *Tric-a*-knockout and wild-type tissues. The cycle threshold (Ct) indicates the cycle number at which the amount of amplified cDNA reaches a fixed threshold in each RT-PCR reaction. (**D**) Maps of the endogenous *Tric-a* gene (EG) and the SMC-specific *Tric-a* transgene (TG). Synthetic primers for PCR analysis are indicated by arrows (for mouse genotyping) and arrowheads (for RT-PCR analysis). A hybridization probe used for Southern blot analysis of *Eco*RI-digested genomic DNAs is indicated by an open box. Transcriptional regions are marked by red boxes. (**E**) PCR genotyping for detection of the transgene in primary founder mice. Tail genomic DNAs from the mice were subjected to PCR using Tg-1 and Tg-2 primers, and amplified DNA fragments were analyzed by agarose gel electrophoresis. DNA fragments derived from the EG and TG are indicated by arrowheads. (**F**) Southern blot analysis of the transgene in founder mice. Tail genomic DNA (10 μg in each lane) was digested with *Eco*RI for blot hybridization using the *Tric-a* cDNA probe. Hybridization-positive DNA fragments derived from EG and TG are indicated by arrowheads. (**G**) RT-PCR detection of *Tric-a* mRNAs derived from EG and TG. Total tissue RNA preparations from at least 3 mice in each genotype were examined by quantitative RT-PCR analysis. Amplified cDNAs were subjected to agarose gel electrophoresis and the representative data are presented. PCR cycle numbers and primer sets used are shown in parentheses (see panel **D**). (**H**) Tail-cuff monitoring of systolic BP and HR in *Tric-a*-knockout mice carrying the transgenic mice. The SMC-specific *Tric-a* transgene seemed to mediate strong hypotensive effects but insufficient HR-elevating effects in *Tric-a*-knockout mice. The data represent the mean ± SEM., and the numbers of mice examined are shown in parentheses. Statistical differences from the values of *Tric-a*-knockout mice are indicated by asterisks (**$p<0.01$ vs. A-/- mice in *t*-test). Primer sets used for DNA amplification are listed in Table S5.

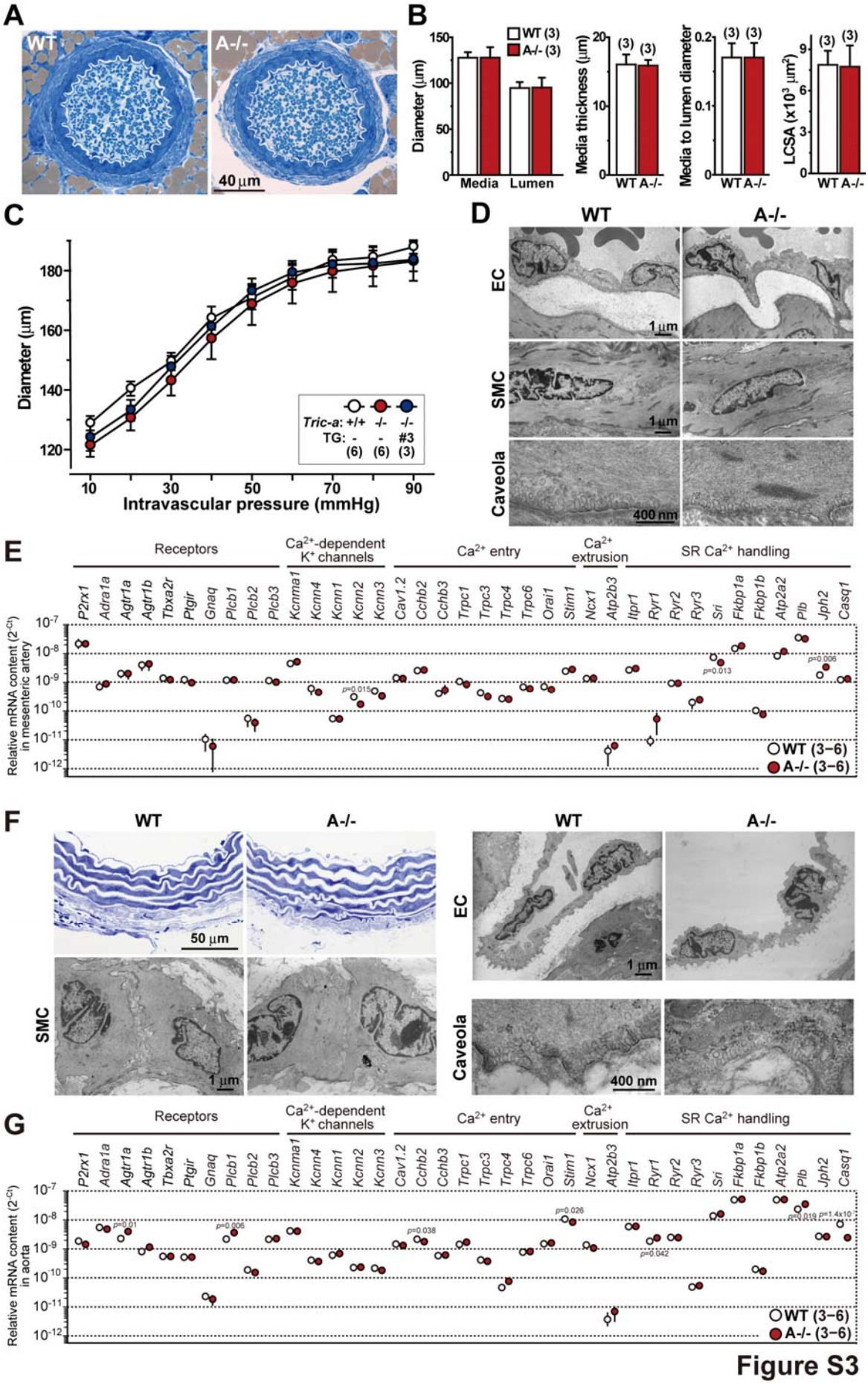

Figure S3

Figure S3. No Signs for Remodeling in *Tric-a*-Knockout Vessels

(**A–E**) Analyses of *Tric-a*-knockout mesenteric arteries. (**A**) Histology of *Tric-a*-knockout arteries. The third branch of the artery was immersed in Ca^{2+}-free PSS supplemented with 4 mM EGTA, and then fixed and embedded in epoxy resin. Thin sections (approximately 1 µm thick) were stained with toluidine blue for light microscopic observation. (**B**) Summarized histological features in *Tric-a*-knockout arteries. The media diameter, lumen diameter, media thickness, media to lumen diameter and lumen cross sectional area (LCSA) of the arterial sections (n>18 from 3 mice) were statistically analyzed using Image J software. (**C**) Passive diameters of arteries at various intravascular pressure levels. The diameter was measured in Ca^{2+}-free Krebs-Ringer solution supplemented with 4 mM EGTA, and the data were summarized. There were no statistical differences within any genotypes. (**D**) Electron-microscopic images of endothelial cells (EC), smooth muscle cells (SMC) and the cell membrane of SMCs (caveola) from mesenteric arteries. Our observations detected no abnormal ultrastructural features in *Tric-a*-knockout mesenteric arteries. (**E**) Quantitative RT-PCR analysis in *Tric-a*-knockout arteries. (**F** and **G**) Analyses of *Tric-a*-knockout thoracic aorta. (**F**) Photo- and electron-microscopic images of endothelial cells (EC), smooth muscle cells (SMC) and the cell membrane of SMCs (caveola) in *Tric-a*-knockout aortas. Our observations detected no abnormal ultrastructural features in the mutant aorta. (**G**) Quantitative RT-PCR analysis in *Tric-a*-knockout aortas. For the data presentation, mRNAs examined are categorized into five groups in **E** and **G**. Primer sets used for cDNA amplification are listed in Table S5. The data represent the mean ± SEM., and the numbers of mice examined are shown in parentheses. Although statistical evaluation detected a few significant differences between genotypes (see *p* values in *t*-test), the changes of mRNA contents seem minimal in *Tric-a*-knockout vessels. Therefore, the overall expression profiles are roughly unchanged between the genotypes. Taken together, we detected no signs of vascular remodeling in *Tric-a*-knockout mice at the young-adult stage.

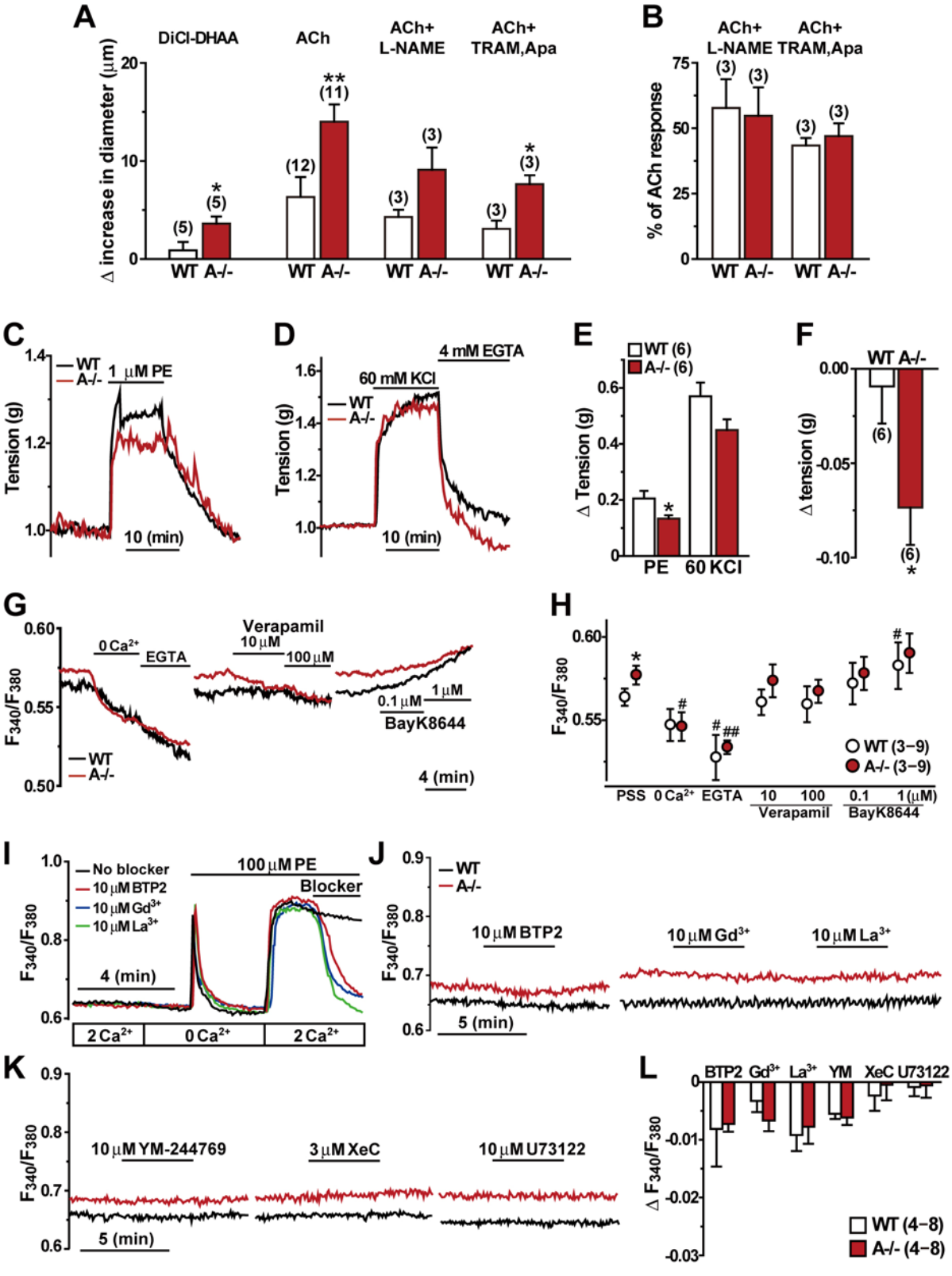

Figure S4

Figure S4. Characterization of Arterial Dilation, Aortic Contraction and Ca^{2+} Handling of VSMC in Tric-a-Knockout Mice

(**A** and **B**) Dilation of mesenteric arteries. Arterial dilation was induced by the BK channel opener 12,14-dichlorodehydroabietic acid (1 μM DiCl-DHAA, refer Sakamoto et al. (2006) J. Pharmacol. Exp. Ther. *316*, 144−153) or acetylcholine (0.1 μM ACh), as measured by diameter monitoring at an intravascular pressure of 70 mmHg. The BK channel opener induced potent vasodilation in *Tric-a*-knockout arteries, suggesting poor activity of BK channels under resting conditions in the mutant VSMCs. ACh-induced vasodilation was also enhanced in *Tric-a*-knockout arteries likely due to elevated myogenic tone under resting conditions in the mutant vessels. To evaluate NO-dependent vasodilation, ACh-induced relaxation was partially inhibited by the NO synthase inhibitor N-nitro-L-arginine methyl ester (100 μM L-NAME). To estimate endothelium-derived hyperpolarizing factor (EDHF)-dependent vasodilation, the relaxation was partially inhibited by the intermediate-conductance Ca^{2+}-dependent K^+ (IK) channel blocker TRAM-34 (10 μM) and the small-conductance Ca^{2+}-dependent K^+ (SK) channel blocker apamin (200 nM). Putative NO- and EDHF-dependent fractional vasodilations were calculated using the original ACh response as a reference. The lack of obvious differences in the fractional values between the genotypes suggests that NO- and EDHF-dependent vasodilations function normally in *Tric-a*-knockout arteries. (**C**−**F**) Contraction of thoracic aorta. (**C** and **D**) Aortic ring preparations were mounted on a fixed isometric force transducer, and resting tension was initially adjusted to 1 g. Contraction was evoked by the α1-agonist phenylephrine (1 μM PE) or 60 mM KCl bathing solution, and relaxation was induced by a Ca^{2+}-free bathing solution. (**E** and **F**) PE and 60 mM KCl-induced contraction and relaxation induced by Ca^{2+} removal were statistically analyzed. *Tric-a*-knockout specimens tended to generate weakened contraction and showed facilitated relaxation in the isometric tension measurements. These observations suggest that the resting myogenic tone is elevated in the mutant aorta. (**G** and **H**) Resting $[Ca^{2+}]i$ of aortic VSMCs. Endothelial cells were removed from aortic preparations and the resulting smooth muscle segments were loaded with Fura-PE3AM for ratiometric Ca^{2+} imaging. Effects of extracellular Ca^{2+} and L-type Ca^{2+} channel modulators on resting $[Ca^{2+}]i$ were examined, and the data obtained are summarized. Resting $[Ca^{2+}]i$ in *Tric-a*-knockout VSMCs was significantly elevated in the presence of extracellular 2 mM $CaCl_2$, but became normal in Ca^{2+}-free and verapamil-containing solutions. In response to BayK8644, resting $[Ca^{2+}]i$ was remarkably elevated in control VSMCs, but not in *Tric-a*-knockout VSMCs. These abnormal characteristics are shared by arterial and aortic VSMCs (see Figure 2). (**I**-**J**) Pharmacological characterization of Ca^{2+} handling in VSMCs. To examine the effects of Ca^{2+}-handling inhibitors, Fura-PE3 Ca^{2+} imaging was carried out in mesenteric artery preparations lacking endothelial cells. Although SOCE evoked in VSMCs was sensitive to authentic SOCE inhibitors, 4-methyl-4′-[3,5-bis(trifluoromethyl)-1H-pyrazol-1-yl]-1,2,3-thiadiazole-5-carboxanilide (BTP2, 10 μM), Gd^{3+} (10 μM) and La^{3+} (10 μM) (**I**), the inhibitors did not attenuate elevated resting $[Ca^{2+}]i$ in *Tric-a*-knockout VSMCs (**J**). Moreover, inhibitors of Na^+-Ca^{2+} exchangers (YM-244769, 10 μM), IP_3 receptors (xestospongin C, 3 μM) and phospholipase C (U73122, 10 μM) exerted no significant effects on resting $[Ca^{2+}]i$ in the mutant VSMCs (**K**). These data are summarized in **L**. The observations suggest no essential contribution of SOCE, Ca^{2+} extrusion or IP_3 signaling to the development of elevated resting $[Ca^{2+}]i$ in *Tric-a*-knockout VSMCs. The data represent the mean ± SEM., and the numbers of mice and experiments from at least 3 mice are shown in parentheses. Statistical differences between the genotypes are indicated by asterisks (*p<0.05, **p<0.01 in t-test). Statistically significant drug-induced effects within each genotype are indicated by sharps (#p<0.05, ##p<0.01 in t-test).

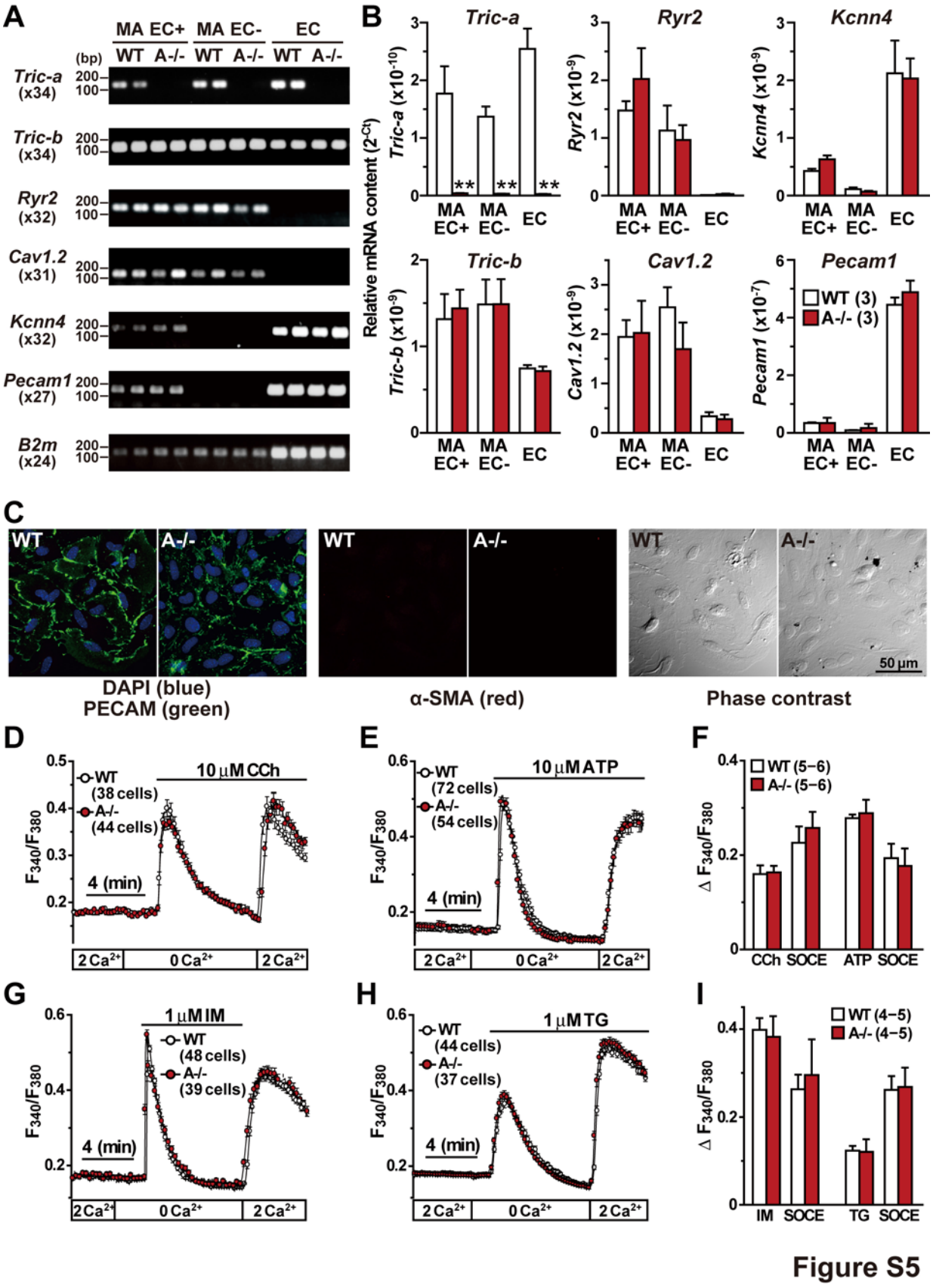

Figure S5

Figure S5. Expression of TRIC Channel Subtypes in Mesenteric Artery, and Normal Ca^{2+} Handling in *Tric-a*-Knockout Endothelial Cells

(**A** and **B**) Quantitative RT-PCR analysis of *Tric-a*, *Tric-b*, *Ryr2*, *Cav1.2*, *Kcnn4* and *Pecam1* mRNAs. Total RNA preparations were extracted from mesenteric arteries (MA) with or without endothelial cells (EC+/-), and primary cultured endothelial cells derived from the aorta (EC). Amplified cDNAs were subjected to agarose gel electrophoresis, and the representative data are presented. RCR cycle numbers are shown in parentheses, and β2-microglobulin mRNA (*B2m*) was examined as an internal control. Primer sets used are listed in Table S5. The cycle threshold (Ct) was determined in each RT-PCR reaction, and the data were statistically examined. (**C**) Immunohistochemical analysis of primary cultured endothelial cells. Immunostaining with antibodies to platelet endothelial cell adhesion molecule (PECAM/CD31, endothelial cell marker) and α-smooth muscle actin (α-SMA, smooth muscle cell marker) confirmed the successful preparation of cultured endothelial cells from the thoracic aorta. (**D**−**I**) Fura-2 ratiometric Ca^{2+} imaging in primary cultured endothelial cells. *Tric-a*-knockout endothelial cells showed normal resting $[Ca^{2+}]i$ and regularly responded to both carbachol (CCh, 10 μM) and ATP (10 μM). Furthermore, after Ca^{2+} release evoked by CCh and ATP, the mutant cells exhibited normal store-operated Ca^{2+} entry (SOCE) (**D**−**F**). Normal SOCE was also detected in the mutant cells, after regular SR Ca^{2+} leak responses induced by ionomycin (IM, Ca^{2+} ionophore, 1 μM) and thapsigargin (TG, Ca^{2+}-pump inhibitor, 1 μM) (**G**−**I**). Our Ca^{2+} imaging detected no abnormal feature in Ca^{2+} handling of *Tric-a*-knockout endothelial cells. The data represent the mean ± SEM., and the numbers of mice and cells examined are shown in parentheses. Statistical differences between the genotypes are indicated by asterisks (**$p<0.01$ in *t*-test).

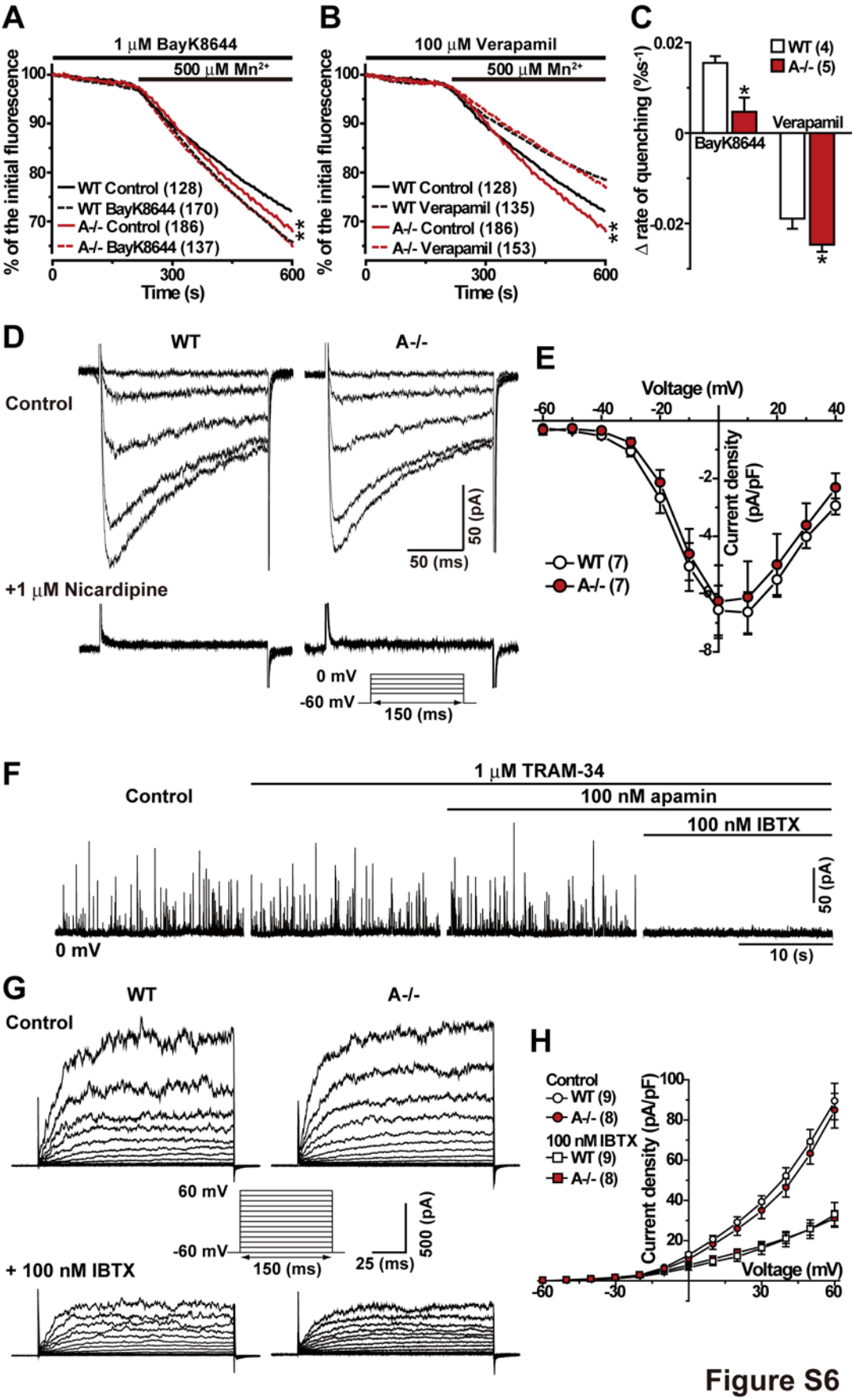

Figure S6

Figure S6. L-type Ca^{2+} Channel and BK Channel Currents in *Tric-a*-Knockout VSMCs

(**A**−**C**) Evaluation of steady-state Ca^{2+} influx by Mn^{2+} quench of Fura-2 fluorescence in VSMCs. Quenching of Fura-2 fluorescence by Mn^{2+} entry was monitored, and effects of BayK8644 (1 μM) and verapamil (100 μM) were examined (**A** and **B**). Averaged time-courses of the quench in *Tric-a*-knockout and control VSMCs are illustrated. Under non-treated conditions, the quench rate in the mutant cells was significantly accelerated, compared with that of wild-type cells. However, similar rates between the genotypes were observed under BayK8644- and verapamil-treated conditions. Therefore, BayK8644 strongly facilitated Mn^{2+} quench in wild-type cells, but not in the mutant cells. In contrast, verapamil-sensitive Mn^{2+} quench was significantly enhanced in the mutant cells (**C**). The observations confirmed our conclusion from Figure 2 that dihydropyridine-sensitive L-type Ca^{2+} channels are hyperactivated under resting conditions in *Tric-a*-knockout VSMCs. (**D** and **E**) L-type Ca^{2+} channel current recording. VSMCs were examined by whole-cell patch clamp using the VDCC pipette solution and depolarized from a holding potential of -60 mV to test potentials. Representative current traces at test potentials of -40, -30, -20, -10 and 0 mV were obtained in the presence and absence of nicardipine (1 μM) (**D**). Currents evoked at test potentials were normalized to membrane capacitance to yield the current density, and the data obtained are summarized as current-voltage relationship curves (**E**). We detected no abnormal characteristics of nicardipine-sensitive currents in *Tric-a*-knockout VSMCs. (**F**−**H**) Ca^{2+}-dependent K^+ channel currents recording. Ca^{2+}-dependent K^+ channels are pharmacologically classified into the following three major groups; apamin-sensitive small-conductance (SK) channels, TRAM-34-sensitive intermediate-conductance (IK) channels and iberiotoxin (IBTX)-sensitive big-conductance (BK) channels. Single VSMCs prepared from wild-type mesenteric arteries were examined in whole-cell patch-clamp recording using the STOC pipette solution at a holding potential of 0 mV. Active STOCs in a control bathing solution were blocked by IBTX (100 nM), but TRAM-34 (1 μM) and apamin (100 nM) did not affect STOC generation (**F**). Therefore, BK channels predominantly mediate STOCs in VSMCs from mesenteric arteries. To evaluate cell-surface BK channel density, VSMCs were examined using the BK pipette solution and depolarized from a holding potential of -60 mV to test potentials in 10 mV steps. Representative current traces before and after IBTX application are shown (**G**). Currents evoked at test potentials were normalized to membrane capacitance to yield the current density, and the data obtained are summarized as current-voltage relationship curves (**H**). We detected no abnormal characteristics of IBTX-sensitive currents in *Tric-a*-knockout VSMCs. The data represent the mean ± SEM., and the numbers of cells and mice examined are shown in parentheses. Statistical differences between the genotypes are indicated by asterisks (*p<0.05, **p<0.01 in *t*-test).

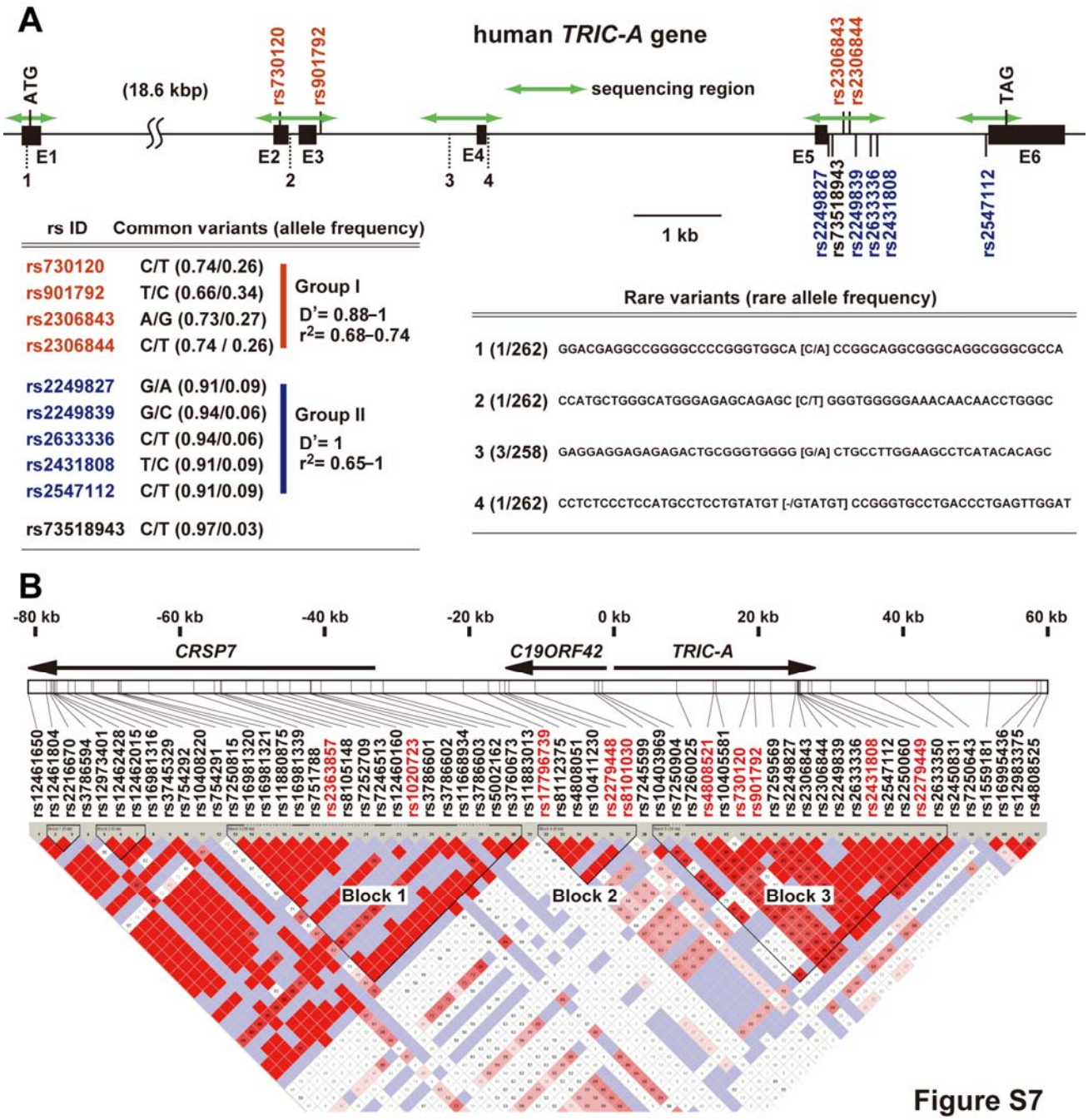

Figure S7. Genetic Variations in Human *TRIC-A* Gene

(**A**) Sequencing of *TRIC-A* segments from 130 Japanese hypertension patients. We sequenced genomic fragments, containing exons (E1−E6) and indicated by green arrows on the gene map, and detected several common variations with rs IDs (left list) and rare variations without rs ID (right list). Most of the common variations are classified into two major groups in linkage disequilibrium; standardized disequilibrium coefficients (*D*') and squared allele-frequency correlations (r^2) are given in each group. Based on the HapMap database and our case-control study, the group-I SNPs (red rs ID) are distributed over 80 kb and associated with a hypertension risk, while the group-II SNPs (blue rs ID) are restricted to 5 kb and showed no correlation with the risk. (**B**) LD mapping analysis of the *TRIC-A* genetic region. The LD plot was produced by analyzing representative SNPs with relatively high frequencies in the HapMap database. The haplotype variations proposed from the database indicate that LD SNPs around the *TRIC-A* gene cluster to form three blocks. The LD SNPs clustered in blocks 2 and 3 largely retained associations with each other in our genotyping analysis, while the SNPs in block 1 do not show high association with the block 2 and 3 LD SNPs. In addition to LD SNPs, there are several non-LD SNPs in these blocks.

Supplemental Tables

Table S1. Clinical Characteristics of Subjects in Case-Control Study

	Hypertensive cases (*n*=1,119)*	Normotensive controls (*n*=1,140)**
Male (%)	49.2	50.8
Age (years)	58.6 ± 10.4	61.3 ± 8.8
Body mass index (kg/m^2)	23.5 ± 2.9	22.3 ± 2.8
Systolic blood pressure (mmHg)	160.5 ± 20.6	111.9 ± 7.8
Diastolic blood pressure (mmHg)	96.9 ± 13.6	69.1 ± 6.8
Antihypertensive medication (%)	58.2	-

*Hypertensive cases: subjects who were treated with antihypertensive medication or who had an SBP more than 160 mmHg and/or a DBP more than 100 mmHg. **Normotensive controls: subjects who had never been treated with antihypertensive medication and who had an SBP less than 120 mmHg and a DBP less than 80 mmHg. The data represent the mean ± SD.

Table S2. Clinical Characteristics of Subjects in GEANE Study

	None (*n*=135)	ARB (*n*=130)	TZD (*n*=124)	CCB (*n*=129)
Male (%)	54.8			
Age (years)	58.4 ± 12.2			
Body mass index (kg/m^2)	23.9 ± 2.8			
SBP (mmHg)	156.0 ± 13.4	134.9 ± 14.3	134.2 ± 14.2	132.9 ± 11.8
DBP (mmHg)	94.3 ± 9.6	83.9 ± 10.0	84.5 ± 9.7	82.6 ± 9.1
MBP(mmHg)	114.9 ± 8.1	100.9 ± 9.6	101.1 ± 9.4	99.4 ± 8.3

The data represent the mean ± SD.

Table S3. *TRIC-A* SNPs and Antihypertensive Therapy

rs ID	genotype	**ARB**	ΔMBP (mmHg)			**TZD**	ΔMBP (mmHg)			**CCB**	ΔMBP (mmHg)		
		frequency	G11	G12+G22	*p*	frequency	G11	G12+G22	*p*	frequency	G11	G12+G22	*p*
rs8112375	CC/CA/AA	7/51/72	-6.1±13.6	-14.6±8.9	0.019	7/49/68	-12.2±13.7	-13.6±8.7	0.692	7/51/71	-7.5±5.7	-15.7±8.9	0.019
rs10403969	AA/AC/CC	7/51/71	-6.1±9.4	-14.5±9.4	0.020	7/49/67	-12.2±8.8	-13.5±9.1	0.706	7/51/70	-7.5±3.5	-15.6±9.0	0.019
rs730120	AA/AG/GG	3/50/76	-11.8±9.4	-14.2±9.4	0.658	3/48/72	-14.6±8.8	-13.5±9.1	0.845	3/50/75	-9.6±3.5	-15.3±9.0	0.273
rs901792	CC/CT/TT	10/57/63	-6.6±12.6	-14.8±8.8	0.007	10/54/60	-7.5±13.2	-14.0±8.4	0.028	11/56/62	-9.2±9.1	-15.8±8.8	0.020
rs7259569	GG/GA/AA	10/57/63	-6.6±12.6	-14.8±8.8	0.007	10/54/60	-7.5±13.2	-14.0±8.4	0.028	11/56/62	-9.2±9.1	-15.8±8.8	0.020
rs17195267	TT/TC/CC	7/49/73	-14.7±11.9	-14.2±9.2	0.888	7/46/72	-17.7±5.7	-13.3±9.1	0.210	7/49/72	-18.5±5.6	-15.1±9.1	0.331
rs8104526	CC/CA/AA	7/51/72	-14.7±11.9	-14.1±9.2	0.876	7/46/71	-17.7±5.7	-13.3±9.1	0.208	7/51/71	-18.5±5.6	-15.1±9.1	0.323
rs773841	CC/CT/TT	7/51/72	-14.7±11.9	-14.1±9.2	0.876	7/46/71	-17.7±5.7	-13.3±9.1	0.208	7/51/71	-18.5±5.6	-15.1±9.1	0.323

The drug-induced effects on MBP were analyzed in SNP genotypes. The data represent the mean ± SD., and statistical differences between the genotypes are indicated by red *p* values.

Table S4. *TRIC-A* SNPs and Antihypertensive Resistance

rs ID	genotype	**ARB**	SBP		DBP		**TZD**	SBP		DBP		**CCB**	SBP		DBP	
		frequency	*β*	*p*	*β*	*p*	frequency	*β*	*p*	*β*	*p*	frequency	*β*	*p*	*β*	*p*
rs8112375	CC/CA+AA	7/123	2.077	0.655	7.043	0.035	7/117	-4.920	0.316	0.551	0.852	7/122	2.865	0.507	5.461	0.070
rs10403969	AA/AC+CC	7/122	1.993	0.667	7.036	0.036	7/116	-5.005	0.308	0.515	0.863	7/121	2.668	0.525	5.408	0.073
rs730120	AA/AG+GG	3/126	-4.650	0.506	1.428	0.776	3/120	-6.728	0.360	-2.299	0.602	3/125	2.032	0.755	1.979	0.660
rs901792	CC/CT+TT	10/120	3.458	0.378	6.361	0.025	10/114	2.461	0.554	5.201	0.037	11/118	1.996	0.568	4.402	0.074
rs7259569	GG/GA+AA	10/120	3.458	0.378	6.361	0.025	10/114	2.461	0.554	5.201	0.037	11/118	1.995	0.568	4.402	0.074
rs17195267	TT/TC+CC	7/122	1.313	0.777	-1.059	0.750	7/118	-2.920	0.552	-4.725	0.105	7/121	0.574	0.894	-4.869	0.103
rs8104526	CC/CA+AA	7/123	1.274	0.783	-1.108	0.738	7/117	-2.889	0.555	-4.732	0.103	7/122	0.528	0.902	-4.908	0.099
rs773841	CC/CT+TT	7/123	1.274	0.783	-1.108	0.738	7/117	-2.889	0.555	-4.732	0.103	7/122	0.528	0.902	-4.908	0.099

Drug-induced depressor effects were evaluated by adjustment for baseline values. Specific depressor effects of minor allele homozygotes are shown as β standardized regression coefficients, and statistical significances are indicated by red *p* values.

Table S5. PCR Primers in the Study

9130011 J15Rik mRNA	For	tggaatgtgttcatgatgctc	*Adra1a* mRNA	For	accattgtcacccagaggag	*Agtr1a* mRNA	For	ggaaacagcttggtggtgat
	Rev	gggaaggtccctggttttc		Rev	atgatggtcagtggcacgta		Rev	acataggtgattgccgaagg
Agtr1b mRNA	For	tacgccaaggaatgatgaca	*Atp2a2* mRNA	For	agttcatccgctacctcatctca	*Atp2b3* mRNA	For	cccctaagatcctcgacctc
	Rev	gtccactacgtccgcaattt		Rev	caccagattgacccagagtaactg		Rev	cttcaggtccaagacgaagc
B2m mRNA	For	ctgaccggcctgtatgctat	*Casq1* mRNA	For	gagcctatgaccatcccaga	*Cav1.2* mRNA	For	tgggttttgggaaattgtgt
	Rev	ccgttcttcagcatttggat		Rev	aaaggcgacaatgtggattc		Rev	cctcattggcttgctctagg
Cchb2 mRNA	For	cagggttctcaaggtgatcaaag	*Cchb3* mRNA	For	ctcccatcatcgtctttgtcaa	*Fkbp1a* mRNA	For	actaggcaagcaggaggtga
	Rev	gaggaacggtgttgggatttt		Rev	gcttatcgtacgccatcatctg		Rev	ctccataggcatagtctgaggagat
Fkbp1b mRNA	For	gagacggaaggacattccctaag	*Gnaq* mRNA	For	aggtggatgtggaaaaggtg	*Itpr1* mRNA	For	ggaccggacaatggaacagat
	Rev	ccctttttgaagcattcctgtgt		Rev	gtccacgtccgtcaggtagt		Rev	catcccgctctgtggtgtaat
Jph2 mRNA	For	aagaagggccgtaaggaagt	*Kcnma1* mRNA	For	aatgcacttcgaggaggcta	*Kcnn1* mRNA	For	tcaaaaatgctgctgcaaac
	Rev	ggccgatgttcagcaagatc		Rev	ctcagccggtaaattccaaa		Rev	tcgttcaccttcccttgttc
Kcnn2 mRNA	For	gatctggcaaagacccagaa	*Kcnn3* mRNA	For	acttcaacacccgattcgtc	*Kcnn4* mRNA	For	ggcacctcacagacacactg
	Rev	gaagtccctttgctgctgtc		Rev	ggaaaggaacgtgatggaga		Rev	tttctccgccttgttgaact
Ncx1 mRNA	For	ggaccaacagctggagagag	*Orai1* mRNA	For	gccagagttactccgaggtg	*P2rx1* mRNA	For	actgggagtgtgacctggac
	Rev	ttctgtaggtgggacgaagg		Rev	cctggtgggtagtcatggtc		Rev	tcccaaacaccttgaagagg
Pecam1 mRNA	For	tgcaggagtccttctccact	*Plb* mRNA	For	tacctcactcgctcggctat	*Plcb1* mRNA	For	cccaagttgcgtgaacttct
	Rev	cagcttcactgctttgcttg		Rev	gatgcagatcagcagcagac		Rev	gttgccaagctgaaaacctc
Plcb2 mRNA	For	acatccaggaagtggtccag	*Plcb3* mRNA	For	caggccagcacagagacata	*Ptgir* mRNA	For	ctacgctttctgctgcctct
	Rev	cgcaccgactcctttacttc		Rev	aggatgctggcaatcaaatc		Rev	agatggaggtcaccaacagg
Ryr1 mRNA	For	attacagagcagcccgaggat	*Ryr2* mRNA	For	ggcagtatggtccggttaga	*Ryr3* mRNA	For	ggccaagaacatcagagtgactaa
	Rev	agaaccttccgcttgacaaact		Rev	caatgccagcaaagtcttga		Rev	tcacttctgccctgtcagtttc
Sri mRNA	For	tggacaggacggacaaattga	*Stim1* mRNA	For	agaatgagaggagccgtcaa	*Tbxa2r* mRNA	For	cctgctcaacaccgttagtg
	Rev	ggcgacaagtctccaggttaaa		Rev	gcctctctgcattttgcttc		Rev	atgacaggtggtgtctgcaa
Tric-a mRNA	For	gtgtccaaggccagcctcat	*Tric-b* mRNA	For	aaggtgatgaatggctgaagatgtc	*Tric-a* EG mRNA	For	gcattcgtcgggcagcgg
	Rev	ccaaacagcactgggcagat		Rev	atgctttgagatcgccaggtg		Rev	gtcggccaggatgtaactcc
Tric-a EG/TG mRNA	For	cttccctgttttcgacctca	*Tric-a* TG mRNA	For	tgaggtcgaaaacagggaag	*Tric-a* TG	For	caggagctgtggagctgtcccg
	Rev	tttacgggcagaaagcagac		Rev	caggaatcctgtgaagcag		Rev	ccggtggcgatcatgatgaacc
Trpc1 mRNA	For	ctcgaaaggcaaggtcaaac	*Trpc3* mRNA	For	ttttccaaatgcaggaggag	*Trpc4* mRNA	For	gcgtgctgctgataacttga
	Rev	agatcttggcgcagttcatt		Rev	gctgatatcgtgttggctga		Rev	cgaagcggaagctagaaatg
Trpc6 mRNA	For	caggcccagattgataagga						
	Rev	ccagctttggctctaacgac						

Supplemental Experimental Procedures

Mutant Mice

Tric-a-knockout mice of C57BL6J and 129 genetic backgrounds were generated and genotyped as described previously (Yazawa et al., 2007). For smooth muscle-specific expression of TRIC-A channels, a transgene was constructed by inserting the mouse *Tric-a* cDNA between the human α-smooth muscle actin promoter (Nakano et al., 1991) and the polyadenylation sequence derived from the pcDNA3.1 expression plasmid (Invitrogen). The transgene was microinjected into fertilized *Tric-a*+/- and *Tric-a*-/- embryos at the single-cell stage, and the embryos were implanted into pseudopregnant foster mice. Transgenic mice were selected by PCR genotyping and Southern blotting, and were crossed with *Tric-a*+/- and *Tric-a*-/- mice. In this study, all of the experiments were predominantly conducted using young-adult male mice (8−12 weeks old), and were conducted with the approval of the Animal Research Committee of Kyoto University according to the regulations on the animal experimentation of Kyoto University.

Blood Pressure and Heart Rate Monitoring

To telemetrically monitor arterial blood pressure (BP), the battery-operated PA-C10 pressure transmitter (Data Sciences International, St Paul, USA.) was implanted into a mouse under anesthesia with pentobarbital (75 mg/kg). The pressure-sensing catheter was inserted into the aortic arch through the right common carotid artery, and the transmitter body was placed in a subcutaneous pouch along the right flank. Following the surgery, the mice were allowed to recover for at least 1 week. Radio signals from the implanted transmitter were captured by the Physiotel RPC-1 receiver (Data Sciences International), and the data were stored online using the Dataquest ART data acquisition system (Data Sciences International). BP was monitored in 10-sec episodes at 5-min intervals for 7 days. For telemetric monitoring of the electrocardiogram, the ETA-F20 radio frequency transmitter (Data Sciences International) was implanted into the peritoneal cavity, and the mouse was allowed to recover for at least 1 week. Radio signals were captured by the RPC-1 receiver, and the recording was acquired at a 1-kHz sampling rate and heart rate (HR) was determined from R-R intervals. BP and HR in the conscious state were also measured by tail-cuff plethysmography (Model BP-98A-L, Softron, Japan), and were evaluated as the average values of 6 trials during daytime. BP and HR shifts were examined before and after intraperitoneal injections of various drugs.

Myogenic Tone Measurements

Arterial diameter measurements were performed as described previously (Iwamoto et al., 2004). Distal mesenteric arteries (2−3 mm length, 120−150 μm passive external diameter) were prepared from mice, cannulated at both ends and continuously superfused with gassed Krebs-Ringer solution at 37 ºC to induce myogenic tone. For diameter monitoring, the arterial outer diameter was continuously monitored by an edge-detection system (National Instruments, Austin, USA. or Scion Corporation, Maryland, USA.).

Ca^{2+} Measurements

To monitor intracellular Ca^{2+} levels ($[Ca^{2+}]i$) in vascular smooth muscle cells (VSMCs) (Iwamoto et al., 2004), the inner surface of the mesenteric artery and thoracic aorta was wiped with gauze to remove endothelial cells in a physiological salt solution (PSS, in mM: 150 NaCl, 4 KCl, 2 $CaCl_2$, 1 $MgCl_2$, 5.6 glucose and 5 HEPES, pH 7.4 with NaOH). The resulting arterial and aortic muscle segments were incubated with 5 μM Fura-PE3AM (Santa Cruz) and 0.02% cremophor EL (Sigma-Aldrich) for approximately 3 hrs at room temperature (~23 ºC). After Fura-PE3 loading, the vascular strip was tightly fixed with fine steel pins onto a silicone rubber sheet, which was placed on a glass-bottom dish. A CCD camera (Sensicam, PCO. imaging, Germany) mounted on the microscope (DM IRB, Leica), equipped with a polychromatic illumination system (MetaFluor ver6.2r6, Molecular Devices), was used to capture the fluorescence images with excitation at 340 and 380 nm, and emission at >510 nm at room temperature. Bathing solutions used were PSS, nominally Ca^{2+}-free PSS (0 Ca^{2+} in Figures 2, S4 and S5) and Ca^{2+}-free PSS containing 4 mM EGTA (EGTA in Figures 2 and S4).

Single VSMC Preparations

Single VSMCs were enzymatically isolated from the mesenteric artery as described previously (Ohi et al., 2001). Arterial preparations were freed from other tissues and fat in Ca^{2+} and Mg^{2+}-free Hanks solution. The tissues were incubated in the Ca^{2+} and Mg^{2+}-free Hanks solution containing 0.2% collagenase (Amano enzyme, Japan), 0.02% papain (Sigma-Aldrich) and 0.3−0.6% bovine serum albumin at 37 ºC for 40 min, and then aggressively suspended using a cut frontal yellow tip to recover isolated VSMCs in Kraft-Bruhe solution (in mM: 70 potassium glutamate, 30 KCl, 10 KH_2PO_4, 1 EGTA, 10 glucose, 10 NaCl, 1 $MgCl_2$ and 10 HEPES, pH 7.2 with N-methyl-D-glucamine).

Ca^{2+} Spark Measurements

For fluorometric Ca^{2+} imaging (Ohi et al., 2001), single VSMCs were seeded onto glass-bottom dishes and incubated with 5 μM Fluo-4AM (Dojindo, Japan) for 20 min at room temperature (~23 ºC) in HEPES-buffered solution (HBS, in mM: 137 NaCl, 5.9 KCl, 2.2 $CaCl_2$, 1.2 $MgCl_2$, 14 glucose and 10 HEPES, pH 7.4 with NaOH). After Fluo-4 loading, fluorescence images with excitation at 488 nm and emission at >520 nm were captured using a total internal reflection fluorescence microscopy system (TE-2000U, Nikon) equipped with an electron-multiplying CCD camera (Hamamatsu Photonics, Japan). The imaging data were analyzed using the custom software Aquacosmos (Hamamatsu Photonics). The intracellular fluorescence intensity was normalized to the baseline intensity to yield the relative intensity (F/F_0). Ca^{2+} spark amplitude is expressed as an increased relative intensity value ($\Delta F/F_0$), and a Ca^{2+} spark was defined as a local fluorescence increase of >0.05 in $\Delta F/F_0$. The frequency was determined from detectable spark generation during a monitoring period.

Mn^{2+} Influx Monitoring

Single VSMCs were seeded onto glass-bottom dishes and incubated with HBS containing 5 μM Fura-2AM (Dojindo) for 30 min at 37 ºC. A CCD camera (Sensicam) mounted on the microscope (DM IRB), equipped with a polychromatic illumination system (MetaFluor ver6.2r6), was used to capture the fluorescence images with excitation at 360 nm, and emission at >510 nm at room temperature (~23 ºC). In the measurements, PSS was used as a standard bathing solution and quenching of Fura-2 fluorescence was induced by Ca^{2+}-free PSS supplemented with 500 μM $MnCl_2$ in the presence and absence of L-type Ca^{2+} channel modulators (Hashii et al., 2000).

Patch-Clamp Recording

Whole-cell voltage clamp recording with patch pipettes (2 to 5 MΩ in pipette resistance and approximately 30 GΩ in seal resistance) was carried out using the Axopatch 200B amplifier (Molecular Device, CA, USA) essentially as described previously (Hotta et al., 2007; Ohi et al., 2001). For spontaneous transient outward current (STOC) monitoring in single VSMC (Figures 3 and S6F), the STOC pipette solution (in mM: 140 KCl, 4 $MgCl_2$, 5 Na_2ATP, 0.05 EGTA and 10 HEPES, pH 7.2 with KOH) and HBS as a bathing solution were utilized. For recording of total Ca^{2+}-dependent K^+ currents (Figure S6G and S6H), the BK pipette solution (in mM: 140 KCl, 1 $MgCl_2$, 6.1 $CaCl_2$, 1 Na_2ATP and 10 EGTA and 10 HEPES, pH 7.2 with KOH, pCa 6.5) and HBS containing 100 μM $CdCl_2$ as a bathing solution were utilized. For recording of voltage-dependent Ca^{2+} channel currents (Figure S6D and S6E), following solutions were used; the VDCC pipette solution (in mM: 120 CsCl, 20 tetraethylammonium, 1 $MgCl_2$, 10 HEPES, 5 EGTA and 2 Na_2ATP, pH 7.2 with CsOH), and the bathing solution (in mM: 30 tetraethylammonium, 1 4-aminopyridine, 107 NaCl, 5.9 KCl, 2.2 $CaCl_2$, 1.2 $MgCl_2$, 14 glucose and 10 HEPES, pH 7.4 with NaOH). All experiments were carried out at room temperature (~23 ºC).

Membrane Potential Monitoring

Single VSMCs were seeded onto glass-bottom dishes and perfused with HBS containing 200 nM oxonol VI (Fluka) for 20 min at room temperature (~23 ºC). During membrane potential recording in the continuous presence of 200 nM oxonol VI, hyperpolarization results in extrusion of the dye from cells to subsequently decrease cellular fluorescence intensity (Apell and Bersch, 1987). To prepare the calibration plot showing the relationship between the fluorescence intensity and membrane potential, HBS solutions containing 20 mM, 30 mM, 60 mM or 140 mM KCl were used as bathing solutions. Fluorescence images with excitation at 559 nm and emission at >606 nm were captured at a sampling rate of ~1.6 s using a confocal microscope system (FV1000, Olympus, Japan) as described previously (Masumiya et al., 2009).

Tension Measurements of Aortic Ring Preparations

Isometric tension of ring preparations from the thoracic aorta (~4 mm in length) was measured as described previously (Iwamoto et al., 2004). Using two thin steel wires, the ring was tied to a force transducer and suspended in Krebs-Henseleit solution (in mM: 118 NaCl, 4.7 KCl, 1.2 KH_2PO_4, 1.2 $MgSO_4$, 2.5 $CaCl_2$, 25 $NaHCO_3$ and 11.7 glucose, pH 7.4 with NaOH) bubbled with 95% O_2 and 5% CO_2 at 37 °C. The ring preparations were stabilized at a resting tension of 1 g for 1 hr before recording contractile responses.

Cultured Endothelial Cells

Endothelial cells were isolated from the thoracic aorta in a collagenase-containing solution and cultured in DMEM supplemented with 20% fetal bovine serum and growth supplements essentially as described previously (Kobayashi et al., 2005). After culturing for 72−96 hrs, endothelial cells were used for immunochemistry and Ca^{2+} imaging. The cells were fixed with 10% formalin for 15 min, treated with a blocking buffer (3% BSA and 0.1% TritonX-100 in PBS) for 10 min, and subjected to immunostaining using anti-mouse CD31 antibody (550274, BD Pharmagen) and anti-human α-smooth muscle actin antibody (ab5694, Abcam). For ratiometric Ca^{2+} imaging, the cells were

loaded with 5 μM Fura-2AM for 45 min at room temperature (~23 ºC) and examined as described previously (Yamazaki et al., 2009).

Anatomical Analysis

Vascular tissues were examined by light and electron microscopes as described previously (Yazawa et al., 2007). The tissues were treated in a fixative solution containing 3% paraformaldehyde, 2.5% glutaraldehyde and 0.1 M sodium cacodylate (pH 7.4), and were postfixed with 1% OsO_4 in the same buffer. The fixed tissues were washed, dehydrated and embedded in epoxy resin. Thin sections (approximately 1 μm thick) were stained with toluidine blue for observation using light microscopy. Ultrathin sections (approximately 80 nm thick) were stained with uranyl acetate and lead citrate, and were examined using an electron-microscope (JEM-1010, JEOL, Japan).

RT-PCR Analysis

For quantitative PCR analysis (Hotta et al., 2007), total RNA preparations from various tissues (at least 3 mice in each genotype) were used as templates for cDNA synthesis (ReverTra ACE qPCR-RT kit, Toyobo, Japan) and analyzed using a real-time PCR system according to the manufacturer's instructions (Thermal Cycler TP800, Takara, Japan). The cycle threshold (Ct) was determined from the cDNA amplification curve as an index for relative mRNA content in each reaction. The PCR primers used in this study are listed in Table S5.

Case-Control Study

Hypertensive cases and normotensive controls were recruited from the Asahikawa, Tokyo, Osaka, and Hiroshima regions of Japan according to the following criteria. Hypertensive subjects (n=758) had a previous diagnosis of hypertension between 30 and 59 years of age, and they were either being treated with antihypertensive medication or had an SBP more than 160 mmHg and/or a DBP more than 100 mmHg. They had a family history of hypertension in their parents and/or siblings and were not obese (BMI less than 25 kg/m^2). Normotensive controls (n=726) aged more than 45 years were recruited from the same regions. These individuals had never been treated with antihypertensive medications and their SBP was less than 120 mmHg and DBP less than 80 mmHg. They had no family history of hypertension. Additional cases and controls were chosen from two population-based samples, the Nomura and Matsuyama cohorts, according to the same criteria. The Nomura study is a longitudinal epidemiological study on Nomura residents, a largely rural community located in Ehime Prefecture (western part of Japan). Subjects were recruited through a community-based annual medical check-up process. Subjects in the Matsuyama cohorts were derived from employees of large manufacturing industries located in Matsuyama, Ehime Prefecture. In all cohorts, clinical parameters were obtained from personal health records during the annual medical check-up process. All study procedures were approved by the ethics committee of each steering university. Signed informed consent was obtained from all participating subjects. Genomic DNAs extracted from blood samples were subjected to SNP genotyping around the *TRIC-A* gene with the TaqMan probe assay using commercially available primers and probes purchased from the Assay-on-Demand system (Applied Biosystems). Frequency differences in each SNP were assessed by the chi-square test, and differences in BP levels among genotypes were assessed using PLINK software (Purcell et al., 2007; http://pngu.mgh.harvard.edu/~purcell/plink/).

GEANE Study

The "GEANE study" (Gene evaluation for antihypertensive effects of drugs study; multicenter clinical trial registry: UMIN-CRT-C000000119) utilized an open random crossover protocol to examine the antihypertensive effects of valsartan (ARB, 80 mg/day), indapamide (TZD, 2 mg/day) and amlodipine (CCB, 5 mg/day). The study subjects (Table S2) were untreated Japanese with essential hypertension (stage 1 and 2 patients with SBP 140−179 mmHg or DBP 90−109 mmHg; see the guideline in the Japanese Society of Hypertension). After informed consent, each drug was prescribed for three months, starting at one half the final does and increasing to the regular dose; the order of the three administered drugs was individually randomized. On the last day of each medication, BP was determined and blood samples were collected for SNP genotyping and regular blood chemical analysis. SNP genotypes were determined with the GeneChip Human Mapping 500K Set. (Affymetrix). The data were examined using the PLINK software in the following two evaluation models; (i) linear regression for differences in BP from pre-medication to post-medication with only SNPs as a fixed effect (Table S3) and (ii) linear regression for post-medication BP with SNPs and pre-medication BP as covariates (Table S4).